

High-Throughput Search for Photostrictive Materials based on a Thermodynamic Descriptor

Zeyu Xiang,^{1,*} Yubi Chen,^{1,2,*} Yujie Quan,¹ and Bolin Liao^{1,†}

¹*Department of Mechanical Engineering,*

University of California, Santa Barbara, CA 93106, USA

²*Department of Physics, University of California, Santa Barbara, CA 93106, USA*

(Dated: August 21, 2024)

Abstract

Photostriction is a phenomenon that can potentially improve the precision of light-driven actuation, the sensitivity of photodetection, and the efficiency of optical energy harvesting. However, known materials with significant photostriction are limited, and effective guidelines to discover new photostrictive materials are lacking. In this study, we perform a high-throughput computational search for new photostrictive materials based on simple thermodynamic descriptors, namely the band gap pressure and stress coefficients. Using constrained density functional theory simulations, we establish that these descriptors can accurately predict intrinsic photostriction in a wide range of materials. Subsequently, we screen over 4770 stable semiconductors with a band gap below 2 eV from the Materials Project database to search for strongly photostrictive materials. This search identifies PtS₂ and Te₂I as the most promising ones, with photostriction exceeding 10⁻⁴ with a moderate photocarrier concentration of 10¹⁸ cm⁻³. Furthermore, we provide a detailed analysis of factors contributing to strong photostriction, including bulk moduli and band-edge orbital interactions. Our results provide physical insights into photostriction of materials and demonstrate the effectiveness of using simple descriptors in high-throughput searches for new functional materials.

Keywords: high-throughput search, photostriction, band gap pressure coefficients, constrained density functional theory

* These authors contributed equally.

† bliao@ucsb.edu

I. INTRODUCTION

Photostriction, defined as the nonthermal mechanical strain of materials when exposed to light, has attracted significant research interests given important applications in photostrictive actuators [1], optical sensors [2], information storage [3], and energy harvesting [4]. Since its discovery in the 1960s, photostriction has been studied in a broad range of semiconductors. In nonpolar semiconductors, such as Si [5] and Ge [6], it is understood that photostriction originates from an “electronic volume effect” (EVE) [7], where the occupation of valence and conduction bands alters chemical bonds and leads to strain. EVE should occur on the time scale of electron-phonon coupling (\lesssim ps) and contributes to photostriction in all semiconducting materials. In polar materials without inversion symmetry, such as zinc-blende [8] and wurtzite [9] polar semiconductors and ferroelectric materials, the inverse piezoelectric effect (IPE) can provide an additional contribution to photostriction. For example, local screening of the polarization by photoexcited carriers in ferroelectrics can lead to ultrafast photostriction on a picosecond time scale due to IPE in ferroelectrics [10, 11]. In addition, macroscopic electron-hole separation induced by a surface photovoltage effect (SPV) in polar semiconductors [8] or a bulk photovoltage (BPV) effect in ferroelectrics can lead to strong photostriction through IPE, which, however, typically occurs on a much slower time scale set by the charge transport process [12]. In these inorganic semiconductors, strain induced by photostriction is typically below 10^{-5} at moderate photocarrier concentrations achievable under continuous laser illumination [13]. Although amorphous chalcogenide glasses and organic semiconductors can exhibit giant photostrictive strain over 1% due to photo-induced bond modification and photoisomerization [14, 15], these effects are usually much slower, taking minutes to hours to finish. Here we make a distinction between “intrinsic” photostrictive effects caused by the presence of uniform photocarriers in the bulk of the sample, e.g. EVE and local polarization screening in ferroelectrics, and “extrinsic” photostrictive effects that rely on macroscopic photocarrier transport and the presence of sample surfaces, e.g. photostriction associated with SPV and BPV effects. Intrinsic photostrictive effects do not require photocarrier transport and, thus, are much faster than extrinsic photostrictive effects, but typically lead to a smaller strain.

In recent years, several materials have been discovered to show giant photostriction resulting from newly proposed mechanisms. For example, the next-generation solar cell material,

methylammonium lead iodide (MAPbI₃), shows significant photostriction, where the light-induced lattice change is $> 0.12\%$ based on atomic force microscope measurements [16, 17]. This effect was attributed to the weakening of hydrogen bonding by photo-induced charge carriers. In addition, strontium ruthenate (SrRuO₃), a transition metal oxide with a perovskite crystal structure, was observed with a 1.12% photo-induced strain based on the Raman peak shifts [18]. The strong light-induced deformation was attributed to the nonequilibrium of phonons in SrRuO₃. Although these experimental discoveries are intriguing and exciting, systematic theoretical guidelines to search for strongly photostrictive materials are still lacking, limiting the efficiency of developing new photostrictive applications.

On the theoretical modeling side, photostriction has recently been studied from first-principles by a constrained density functional theory (c-DFT) method [19], through which a fixed electron concentration is excited from a chosen valence band state to a specific conduction band state [11] and the lattice is allowed to relax with the electron occupation as a constraint. The resulting lattice change along selected crystal directions as a result of the photoexcited electron-hole pairs is evaluated as photostriction. This method was applied to study photostrictive coefficients in ferroelectric materials [11, 20], where it was shown to accurately capture the EVE and the polarization screening contributions to photostriction (the intrinsic photostriction), while the extrinsic photostriction caused by macroscopic charge separation cannot be modeled since a spatially uniform distribution of electron-hole pairs is assumed in c-DFT simulations. c-DFT has also been applied successfully to model photostriction in halide perovskites [21]. These results suggest that c-DFT can be used as an effective benchmark calculation of intrinsic photostrictive effects for semiconductors, but its relatively high computational cost prohibits its use to broadly screen and discover new materials with a strong photostriction.

In this work, we conduct a high-throughput search for strongly photostrictive materials based on a thermodynamic descriptor, the band gap pressure or stress coefficient, which can be efficiently evaluated by ground-state DFT calculations. The band gap pressure coefficient was connected to the photostriction coefficient in early studies [6]. Here, we provide a derivation based on thermodynamic Maxwell relations and generalize the result to materials with anisotropic photostriction, where the band gap stress coefficient is more relevant. We then verify that these thermodynamic descriptors can be used to accurately predict the intrinsic photostrictive effects in a broad range of materials by comparing to c-DFT simu-

lations [19]. Encouraged by this result, we compute the band gap pressure coefficients of 4770 semiconducting materials (band gap within 2 eV) using DFT to search for new photostrictive materials. Among these materials, the band gap pressure coefficient of PtS₂ is found to be the highest (-49.17 meV/kB), whose photostrictive strain along the out-of-plane direction is nearly 18 times higher than that of MAPbI₃ with an identical photoexcited electron concentration. Upon closer examination of materials exhibiting substantial band gap pressure/stress coefficients, it becomes apparent that those with a longer bond length tend to display higher photostriction given the rapid decrease of their bulk moduli. Furthermore, a simplified linear combination of atomic orbitals (LCAO) analysis coupled with the crystal orbital Hamilton population (COHP) method [22, 23] is subsequently utilized to compare photostriction among materials exhibiting similar bulk moduli. It is found that materials with band edges formed by cations and anions with a small orbital energy difference tend to exhibit high deformation potentials that lead to a strong photostriction. Our work identifies several new strongly photostrictive materials for potential applications and provides systematic guidelines for understanding photostriction in a wide range of semiconductors.

II. THEORY AND METHODS

A. Thermodynamics of Intrinsic Photostriction

In the early literature, intrinsic photostriction was heuristically linked to the band gap pressure coefficient in isotropic materials [6]. Here, we provide a simple thermodynamic argument to derive this result and generalize it to anisotropic materials, where photo-induced strains along different crystallographic directions are distinct. We focus only on intrinsic photostriction caused by the presence of uniform photocarriers and electron-phonon coupling. Technically, accurate modeling of extrinsic photostriction requires a description of macroscopic photocarrier transport, which is highly complex and not suitable for a high-throughput study. Practically, intrinsic photostriction occurs on a much faster timescale (controlled by electron-phonon interaction) than extrinsic photostriction (limited by photocarrier transport) and is, thus, more suitable for many applications. In addition, since all semiconductors exhibit intrinsic photostriction, our result examines the lower limit of achievable photostriction, whereas extrinsic photostriction in certain groups of semiconductors can

further increase the photo-induced strain.

First, the change of the Gibbs free energy of a unit cell with electrons photoexcited from the valence band maximum (VBM) to the conduction band minimum (CBM) can be expressed as:

$$dG = V dp - S dT + (\mu_e - \mu_h) dn, \quad (1)$$

where V is the unit cell volume, p is the pressure, S is the entropy, T is the temperature, μ_e (μ_h) is the quasi-Fermi level of photoexcited electrons (holes), and n is the number of photoexcited electron-hole pairs per unit cell (assuming photoexcited electrons and holes have the same concentration). $\mu_e - \mu_h$ determines the open-circuit voltage generated by a semiconductor under light illumination [24].

According to the Maxwell's relation, the partial derivative of volume with respect to the excited electron number at a constant pressure $\left(\frac{\partial V}{\partial n}\right)_p$ is equal to the change of the open-circuit voltage with respect to pressure at a constant photocarrier concentration $\left(\frac{\partial(\mu_e - \mu_h)}{\partial p}\right)_n$:

$$\left(\frac{\partial V}{\partial n}\right)_p = \left(\frac{\partial(\mu_e - \mu_h)}{\partial p}\right)_n. \quad (2)$$

This relation suggests that how the open-circuit voltage evolves with increasing pressure at a constant photocarrier concentration can be used to predict the photostrictive behavior of materials. Since c-DFT examines the photostriction of materials at the ground state ($T = 0$ K), where the open-circuit voltage approaches the band gap E_G , $\left(\frac{\partial(\mu_e - \mu_h)}{\partial p}\right)_n$ can be evaluated by the band gap pressure coefficient $\alpha_p = \left(\frac{\partial E_G}{\partial p}\right)_n$. Namely, if we define a volumetric photostriction coefficient $V_n = \left(\frac{\partial V}{\partial n}\right)_p$, it can be evaluated using the band gap pressure coefficient under a constant photocarrier concentration:

$$\left(\frac{\partial V}{\partial n}\right)_p = \left(\frac{\partial E_G}{\partial p}\right)_n, \quad (3)$$

which can be efficiently computed using ground-state DFT.

More generally, photostriction can vary along different lattice directions in anisotropic materials, which leads us to rewrite the change of Gibbs free energy from Eq. 1 into the strain-stress form:

$$dG = \sum_{ij} \epsilon_{ij} V d\sigma_{ij} - S dT + E_G dn, \quad (4)$$

where ϵ_{ij} and σ_{ij} refer to the strain and stress tensor components along three Cartesian directions, respectively. Here, the stress σ_{ij} refers to the internal stress developed in the

material as a response to an external load. Similarly, we define a linear photostriction coefficient as the partial derivative of a strain component along a specified lattice direction with respect to the photoexcited electron concentration $\epsilon_n = V \left(\frac{\partial \epsilon_{ij}}{\partial n} \right)_\sigma$, which can then be related to the variation of the band gap with stress along the corresponding lattice direction $\alpha_s = \left(\frac{\partial E_G}{\partial \sigma_{ij}} \right)_{n, \text{other } \sigma_{ij}}$ under a constant photoexcited carrier concentration:

$$V \left(\frac{\partial \epsilon_{ij}}{\partial n} \right)_\sigma = \left(\frac{\partial E_G}{\partial \sigma_{ij}} \right)_{n, \text{other } \sigma_{ij}}, \quad (5)$$

where $\left(\frac{\partial \epsilon_{ij}}{\partial n} \right)_\sigma$ is evaluated with a constant stress along all directions (experimentally, stress-free condition along all directions), while $\left(\frac{\partial E_G}{\partial \sigma_{ij}} \right)_{n, \text{other } \sigma_{ij}}$ is evaluated when all other nonequivalent stress components are held constant. For brevity, we use $\left(\frac{\partial E_G}{\partial \sigma_{ij}} \right)_n$ in the remainder of this paper. In this work, we focus on photostrictive behaviors along the three main diagonal directions ($ij = xx, yy, zz$), which are relevant for materials with tetragonal and orthorhombic symmetries.

B. Computational Methods

DFT calculations were accomplished via the Vienna ab initio simulation package (VASP) [25, 26] based on the projected augmented wave (PAW) pseudopotentials [27]. The Perdew-Burke-Ernzerhof form of generalized gradient approximation (PBE-GGA) [28] was used for structural optimization. For materials studied in this paper, \mathbf{k} -point convergence and plane-wave cut-off energy convergence were first tested to ensure that the lattice parameters were well relaxed. For example, for the calculation of MAPbI₃, the plane-wave cutoff energy was set at 520 eV and the energy and force convergence criteria were set to 1×10^{-8} eV and 5×10^{-4} eV/Å, respectively. The Γ -centered $7 \times 4 \times 4$ \mathbf{k} -point grids were used to sample the first Brillouin zone.

The c-DFT method [19] was used to simulate materials with a fixed concentration of photoexcited electrons, where the occupations of electronic states near the band edges were imposed as a constraint during the DFT simulation and lattice relaxation. To evaluate the first correlation $\left(\frac{\partial V}{\partial n} \right)_p = \left(\frac{\partial E_G}{\partial p} \right)_n$, lattices were relaxed with different photocarrier concentrations under linearly distributed hydrostatic pressures, where the change of volume as a function of the photocarrier concentration was evaluated as the volumetric photostriction

coefficient at a given pressure. On the right-hand side, the band gap was evaluated as a function of pressure at given photocarrier concentrations. To evaluate the second correlation in anisotropic materials $V \left(\frac{\partial \epsilon_{ij}}{\partial n} \right)_\sigma = \left(\frac{\partial E_G}{\partial \sigma_{ij}} \right)_n$, lattice relaxation was performed with different photocarrier concentrations to minimize stress along all directions. This constraint also corresponds to typical experimental conditions measuring photostriction of a stress-free sample. Lattice changes along different directions as a result of the relaxation were evaluated as the directional photostriction coefficients. On the right-hand side, the band gap was evaluated as a function of stress applied along one direction, while the lattice was relaxed to minimize stress along the other directions.

The bonding nature associated with electron energy bands was analyzed by the COHP method [22], which decomposes the energy of the electronic band structure into interactions (overlaps) between pairs of atomic orbitals between adjacent atoms. In other words, COHP analysis provides a bond-weighted electronic density of states and provides a quantitative measure of the bonding and anti-bonding contributions to the electronic bands, especially near the band extrema. In a COHP analysis, typically a positive (negative) sign corresponds to anti-bonding (bonding) interactions. Conventionally, COHP diagrams plot the negative value (-pCOHP), therefore making bonding (anti-bonding) states on the right (left) of the axis for intuitive visualization [23].

For high-throughput search of new materials with significant photostriction, we selected 4770 stable materials with band gaps in the range of 0-2 eV (calculated by DFT-PBE) from the Materials Project database [29]. A plane-wave cutoff energy of 400 eV was first utilized for the lattice relaxation of all materials to be screened, followed by band gap calculations under three different pressures [2 kilobar (kB), 6 kB, and 10 kB]. The extracted band gap pressure coefficients are then used to discover materials with potentially strong photostriction. For promising material candidates, further \mathbf{k} -point and plane-wave cutoff energy convergence were tested to ensure the convergence of the lattice parameters and forces, followed by COHP analysis of the bonding characteristics. For example, the plane-wave cutoff energy was 500 eV and 600 eV for Te₂I and PtS₂, with energy and force convergence criteria set to 1×10^{-8} eV and 1×10^{-4} eV/Å, and 1×10^{-10} eV and 5×10^{-6} eV/Å., respectively. Correspondingly, the Γ -centered $8 \times 2 \times 2$ and $11 \times 11 \times 6$ \mathbf{k} -point grids were used to sample the first Brillouin zone of the two materials.

III. RESULTS AND DISCUSSIONS

A. Verification of Thermodynamic Descriptor for Isotropic and Anisotropic Materials

We first performed simulations to verify that the thermodynamic descriptors, i.e. the band gap pressure and stress coefficients in Eqn. 3 and Eqn. 5, can indeed be used to accurately predict the photostrictive coefficients in isotropic and anisotropic materials evaluated by c-DFT. Several representative isotropic materials including Si (lattice parameter 5.47 Å, non-polar), PbTe (lattice parameter 6.54 Å, polar), and GaAs (lattice parameter 5.75 Å, polar) were first studied. To stay in the linear regime where Maxwell's relation is valid, the number of excited electrons at a single \mathbf{k} -point (at the VBM) per unit cell was limited to be less than 2 across materials (corresponding to a photocarrier concentration below 10^{20} cm⁻³), with the imposed hydrostatic pressure varying from 0 to 5 kB. The difference of \mathbf{k} -point weights between VBM and CBM was considered for Si given the indirect band gap. The number of excited electrons at VBM per unit cell n is transformed into an excited electron density n_e after considering the \mathbf{k} -point weight at VBM and the unit cell volume. Figure 1a shows how the band gap changes with the hydrostatic pressure in the presence of different excited electron densities (marked by different shades of the symbols) for Si, PbTe, and GaAs. Band gap pressure coefficients $\alpha_p = \left(\frac{\partial E_G}{\partial p}\right)_n$ were fitted as -1.96 meV/kB, -4.70 meV/kB, and 11.85 meV/kB for Si, PbTe, and GaAs, respectively, and compared with previous experiments and calculations (-1.41 meV/kB [30], -1.90 meV/kB [31] for Si; -7.40 meV/kB [32] and -4.01 meV/kB [33] for PbTe; 12.60 meV/kB [30] and 9.8 meV/kB [31] for GaAs). Notably, GaAs shows a positive band gap pressure coefficient, while Si and PbTe show negative band gap pressure coefficients. GaAs is a direct band gap semiconductor with strong covalent bonds, whose band gap is formed between a bonding valence band and an antibonding conduction band. In this case, an applied pressure reduces the interatomic distance and enhances the bonding-antibonding interaction, thus increasing the band gap [31]. In contrast, PbTe is a direct band gap semiconductor with an antibonding VBM [33, 34], therefore reduced interatomic distance raises the VBM energy and reduces its band gap. On the other hand, Si is an indirect band gap semiconductor, whose band gap shrinks under pressure likely due to a broadened width of the conduction band [31]. Figure 1b presents the

developed strain by excited electron densities at different hydrostatic pressures for the three materials, from which the values of volumetric photostriction coefficients $V_n = \left(\frac{\partial V}{\partial n}\right)_p$ were determined as -1.98 meV/kB (Si), -4.98 meV/kB (PbTe), and 11.34 meV/kB (GaAs), respectively. A direct comparison of these results to experimentally measured photostriction is difficult due to the uncertainty in estimating the photocarrier concentration achieved in experiments. Assuming a moderate photocarrier concentration of $10^{17\sim 18} \text{ cm}^{-3}$, our predicted linear photostriction of selected materials is summarized in Table I. Here the linear photostriction $\frac{\Delta L}{L}$ for isotropic materials is determined by $\frac{1}{3} \frac{\Delta V}{V}$. For Si, a negative photostriction (photoinduced contraction) on the order of 10^{-7} is in agreement with experiments [5]. GaAs and CdS show positive photostriction (photo-induced expansion) with coefficients slightly higher than Si in our simulation. Photo-induced expansion in GaAs and CdS were experimentally observed [8, 9], but it is hard to compare the absolute magnitude due to extrinsic contributions from the SPV effect and thermal expansion, in addition to unknown experimental photocarrier concentrations. Importantly, however, the close agreement between α_p and V_n in our simulations confirms that the band gap pressure coefficient can be used to accurately predict the intrinsic volumetric photostriction coefficient in isotropic materials evaluated by c-DFT.

Table I. Predicted photostriction of selected materials at a photocarrier concentration of 10^{17} cm^{-3} to 10^{18} cm^{-3} .

	Simulated Photostriction, $\Delta L/L$
Si	$-1.1 \times 10^{-7\sim -6}$
GaAs	$6.3 \times 10^{-7\sim -6}$
CdS	$2.1 \times 10^{-7\sim -6}$
BaTiO ₃ (z-direction)	$-1.1 \times 10^{-7\sim -6}$
MAPbI ₃ (x-direction)	$-1.6 \times 10^{-6\sim -5}$
MAPbI ₃ (y-direction)	$-2.0 \times 10^{-6\sim -5}$
MAPbI ₃ (z-direction)	$1.5 \times 10^{-6\sim -5}$
Te ₂ I (z-direction)	$-1.0 \times 10^{-5\sim -4}$
PtS ₂ (z-direction)	$-2.7 \times 10^{-5\sim -4}$

Anisotropic materials like GaN (wurtzite, $a, b = 3.22 \text{ \AA}, c = 5.24 \text{ \AA}$), MAPbI₃ (orthorhombic, $a, b, c = 8.56, 9.32, 12.92 \text{ \AA}$), polythiophene (PT) molecular crystal (orthorhombic, $a, b, c = 8.62, 6.00, 7.81 \text{ \AA}$) [35] and BaTiO₃ (tetragonal, $a, b, c = 3.99 \text{ \AA}, 3.99 \text{ \AA}, 4.10 \text{ \AA}$) were subsequently investigated to verify the thermodynamic relation given in Eqn. 5. The crystal structures and orientations of these materials are shown in Supplementary Material Section I.A. In these materials, photo-induced strain can vary significantly along different directions, therefore the volumetric photostriction coefficient alone is insufficient to fully describe the photo-induced strain state. The lattice structures were first relaxed under different hydrostatic pressures with the same step as isotropic materials to account for the photo-induced strain along different directions $\epsilon_n = V \left(\frac{\partial \epsilon_{ij}}{\partial n} \right)_\sigma$. Then the band gap stress coefficient $\alpha_s = \left(\frac{\partial E_G}{\partial \sigma_{ij}} \right)_n$ was calculated by imposing strain along a specific direction (in the range of 0 to 0.02) and evaluating the corresponding stress along that direction while relaxing the stress along other directions with different excited electron numbers at VBM per unit cell (0 to 2). Figure 1c shows the band gap change in these materials with stress along the out-of-plane (σ_z) direction with different excited electron densities for GaN, MAPbI₃, PT, and BaTiO₃ (results along the in-plane direction for GaN and MAPbI₃ are provided in Supplementary Material Section II.B. and II.C.). The band gap stress coefficients $\alpha_s = \left(\frac{\partial E_G}{\partial \sigma_z} \right)_n$ along the out-of-plane direction for GaN, MAPbI₃, PT, and BaTiO₃ were fitted as 2.68 meV/kB, 9.32 meV/kB, -1.28 meV/kB, and -0.75 meV/kB, respectively. Although it was previously reported that the band gap of MAPbI₃ was reduced with an increasing hydrostatic pressure [36], the positive out-of-plane ϵ_n here is not contradicting the previous result due to the anisotropic response. Figure 1d depicts the corresponding strain change with excited electron densities, and the linear coefficients of photostriction $\epsilon_n = V \left(\frac{\partial \epsilon_z}{\partial n} \right)_\sigma$ were calculated as 2.56 meV/kB (GaN), 9.32 meV/kB (MAPbI₃), -1.31 meV/kB (PT), and -0.69 meV/kB (BaTiO₃), accordingly. The results are summarized in Table I. For MAPbI₃ exposed to light, the out-of-plane direction expands and the photostriction evaluated here is $1.5 \times 10^{-6 \sim -5}$ for a photocarrier concentration of 10^{17} to 10^{18} cm^{-3} , close to the experimental measurements of 5×10^{-5} in a bulk MAPbI₃ crystal [16]. However, its in-plane lattice contracts under light with a photostriction on the order of $2 \times 10^{-6 \sim -5}$. In tetragonal BaTiO₃, the out-of-plane direction refers to the polarization direction, and 10^{-4} compression of the polar axis under visible light was previously observed experimentally [37]. Here, we also predict a lattice contraction along the polarization direction of BaTiO₃, but the order of magnitude is hard

to compare considering the uncertainties in estimating the photocarrier concentration.

Figure 2 summarizes the results comparing the photostriction coefficients simulated by *c*-DFT to the band gap pressure or stress coefficients evaluated by DFT for selected isotropic materials (Si, GaAs, CdTe, CdS, PbTe, ZnSe) and anisotropic materials (GaN, MAPbI₃, PT, BaTiO₃). Detailed simulation results of these materials are provided in the Supplementary Material. Among these materials, GaAs presents the highest band gap pressure coefficient of 11.85 meV/kB. ZnSe and CdTe possess band gap pressure coefficients of 7.58 meV/kB and 8.28 meV/kB, corresponding to a relatively large photostriction compared with CdS, whose band gap pressure coefficient is 4.14 meV/kB. The slopes of band gap change with stress in *x*- and *y*-directions for orthorhombic MAPbI₃ are -10.47 and -13.40 meV/kB, indicating a lattice contraction under light illumination in these two directions. The close agreement between the band gap pressure (stress) coefficient and photostriction coefficient, as presented in Figs. 1 and 2, suggests that the thermodynamic relation summarized in Eqns. 3 and 5 is widely applicable to predict the intrinsic photostriction in a broad range of non-polar, polar, ferroelectric, and organic semiconductors.

B. High-throughput Search of Materials with Promising Photostriction

Following the validation of using the thermodynamic descriptors, i.e. band gap pressure and stress coefficients, to predict intrinsic photostriction coefficients, we conducted a high-throughput computational search of potential materials exhibiting significant photostriction thanks to the fact that the band gap pressure coefficients can be efficiently evaluated at the ground-state DFT level. We selected 4770 stable materials with band gaps ranging from 0 to 2 eV (as calculated by PBE DFT) from the Materials Project database [29]. Subsequently, the lattice structures were relaxed under a series of externally applied pressures (2 kB, 6 kB, and 10 kB), through which the band gap pressure coefficients were determined by linear fitting. A screened list of the top 500 photostrictive materials is provided in Supplementary Material Section III.B. Table II lists the band gap pressure coefficients and the relatively low bulk moduli (compared to the Si bulk modulus of 980 kB) of the top 20 materials, highlighting the crucial role of the latter in impacting the photostrictive behaviors of materials. This aligns well with the physical intuition that materials with low bulk moduli are more easily distorted, which could be one indicator for strong photostriction. In addition,

we also analyzed the bonding nature of the VBM of these materials using the COHP method, which is also listed in Table II. Interestingly, we found that most materials with a large band gap pressure coefficient in our search exhibit an antibonding valence band. This observation suggests that an antibonding valence band may lead to a higher sensitivity of the band gap to external pressure or stress, and thus strong photostriction. Intuitively, occupied antibonding valence bands create instability in the lattice [34], and photoexcitation from antibonding valence bands may temporarily improve the stability of the lattice, leading to a large photostriction in the process.

Among these materials of interest, PtS₂ and Te₂I present notably high band gap pressure coefficients of -49.17 meV/kB and -48.53 meV/kB, approximately 4 times that of MAPbI₃. PtS₂ was previously synthesized and reported to have a CdI₂ structure, where each layer of the crystal is composed of a two-dimensional close-packed arrangement of metal atoms situated between two layers of chalcogen atoms [38–40]. Te₂I belongs to tellurium subhalides based on the substoichiometric halogen element, of which the crystalline structure is coordinated by threefold screw axis of Te element and shows interchain van der Waals (vdW) interactions [41]. This material was first made through hydrothermal synthesis [42]. Considering their anisotropic and layered structures, we performed a detailed analysis of the out-of-plane photostriction for both materials. Their crystal structures and directions are shown in Supplementary Material Section I.B. Figure 3a and 3c show that the band gap of Te₂I and PtS₂ decreases with stress σ_z and the coefficients are -71.24 meV/kB and -173.46 meV/kB, respectively. Figure 3b and 3d present photo-induced lattice contraction of Te₂I and PtS₂ along the corresponding out-of-plane direction, where considerable photostriction coefficients are extracted as -63.73 meV/kB and -166.86 meV/kB (approximately 7 times and 18 times higher than MAPbI₃'s 9.32 meV/kB). The small difference between the band gap stress coefficient and the photostriction coefficient for both Te₂I and PtS₂ once again demonstrates the robustness of the thermodynamic relations (Eqns. 3 and 5) in predicting photostriction in materials. Despite similar band gap pressure coefficients, the lattice of PtS₂ contracts significantly more along the out-of-plane direction compared to that of Te₂I under light illumination. Coefficients of photostriction of PtS₂ and Te₂I along the out-of-plane direction with a photocarrier concentration of 10^{17} cm⁻³ to 10^{18} cm⁻³ are $-2.7 \times 10^{-5 \sim -4}$ and $-1.0 \times 10^{-5 \sim -4}$, respectively, and compared to other materials in Table I. These photostriction coefficients are an order of magnitude higher than MAPbI₃ and two orders of

Table II. Band gap pressure coefficients, bulk moduli, and VBM bonding type of the top 20 photostrictive materials discovered in our search.

	Band gap Pressure Coefficient, (meV/kB)	Bulk Modulus, (kB)	VBM, Bonding Type
PtS ₂	-49.17	71.84	anti-bonding
Te ₂ I	-48.53	95.14	anti-bonding
ScI ₃	-39.59	53.32	anti-bonding
HgI	-39.23	106.35	anti-bonding
Te ₂ Br	-38.71	106.45	anti-bonding
AsS	-38.30	60.35	anti-bonding
PdSe ₂	-35.78	148.48	anti-bonding
WS ₂	-33.71	104.23	weak bonding
PdS ₂	-33.54	123.37	anti-bonding
PAuS ₄	-33.23	51.91	anti-bonding
WSe ₂	-33.01	87.52	weak bonding
SiAs	-32.82	107.85	anti-bonding
Cs ₂ Se ₅	-32.26	77.60	anti-bonding
AuSe	-31.59	94.04	anti-bonding
PI ₂	-31.26	52.28	anti-bonding
InS	-31.14	165.11	anti-bonding
AsSe	-30.78	69.66	anti-bonding
MoSe ₂	-30.12	98.16	weak bonding
InSe	-29.78	109.33	weak bonding
TlBr ₂	-29.77	112.85	anti-bonding

magnitude higher than Si. The remarkably large photostriction of PtS₂ and Te₂I defies the conventional impression that the intrinsic photostriction of inorganic bulk semiconductors is below 10⁻⁵. The extraordinary photostriction of PtS₂ and Te₂I suggests their potential for advanced optomechanical applications.

C. Physical Insights into Giant Photostriction

According to the thermodynamic relation (Eqn. 3 and 5), materials exhibiting giant intrinsic photostriction should also possess large band gap pressure coefficients α_p , which can be expressed as [31]:

$$\alpha_p = \left(\frac{dE_G}{dp} \right)_n = -\frac{1}{B} \left(\frac{dE_G}{d \ln V} \right)_n = -\frac{1}{B} \alpha_v \quad (6)$$

where $B = -\frac{dp}{d \ln V}$ is the bulk modulus and $\alpha_v = \frac{dE_G}{d \ln V} = \frac{dE_C}{d \ln V} - \frac{dE_V}{d \ln V}$ is the band gap volume coefficient, which is determined by the difference between the deformation potentials associated with CBM ($\frac{dE_C}{d \ln V}$) and VBM ($\frac{dE_V}{d \ln V}$) (E_C and E_V are the electronic energies of the CBM and VBM, respectively). A list of the band gap pressure and volume coefficients of semiconductors studied here is provided in Table III. Equation 6 illustrates that a small bulk modulus, coupled with a significant difference in the deformation potentials between CBM and VBM, can lead to a substantial band gap pressure coefficient and, thus, a strong photostriction. An analysis of materials included in our high-throughput screening reveals that the band gap pressure coefficient exhibits a generally decreasing trend with an increasing bulk modulus, which in turn decreases with an increasing bond length (see Fig. S9 in the Supplementary Material). However, bulk modulus is not the sole factor - the band gap pressure coefficients of materials with similar bond lengths can still vary by two orders of magnitude due to the difference in their deformation potentials. Wei and Zunger [31] adopted a simplified LCAO model to analyze the deformation potential associated with the band edges:

$$E_{V/C} = \frac{\mu^c + \mu^a}{2} \mp \sqrt{\left(\frac{\mu^c - \mu^a}{2} \right)^2 + M^2} \quad (7)$$

where μ^c and μ^a are isolated cation and anion orbital energies before hybridization, respectively, $-$ and $+$ represent bonding and anti-bonding interactions, and M is the matrix element between orbitals and inversely proportional to the bond length l as $M \sim l^{-2}$ [43]. Taking a derivative of the volume $V \sim l^3$, the deformation potential for VBM and CBM based on Eqn. 7 is given by:

$$\alpha_v^{VBM/CBM} \sim \mp \frac{M^2}{\sqrt{\left(\frac{\mu^c - \mu^a}{2} \right)^2 + M^2}}, \quad (8)$$

which implies the magnitude of the deformation potential becomes larger when the orbital energy difference $\mu^c - \mu^a$ decreases. Figure 4a compares the predicted magnitude of photo-

striction based on the band gap pressure coefficient (left y-axis) and the bulk moduli (right y-axis) among Si, MAPbI₃, HgI, ScI₃, Te₂I, and PtS₂, indicating that a relatively low bulk modulus is crucial for a significant photostriction. This is consistent with our physical intuition, as materials with lower bulk moduli are more prone to distortion under external loads. For MAPbI₃, Te₂I, and PtS₂ with comparable bulk moduli, the deformation potentials become essential when comparing the photostriction coefficient. Figure 4b-d show the strongest anti-bonding interactions near VBM for these three materials based on COHP analyses. The orbital energy differences for Te₂I ($\mu^{Te5p} - \mu^{Te5p}$) and PtS₂ ($\mu^{Pt5d} - \mu^{S3p}$) are relatively smaller compared to MAPbI₃ ($\mu^{I5p} - \mu^{Pb6s}$), leading to remarkably larger photostriction coefficients.

Based on the analysis presented above, we summarize our findings according to Table III, some of which follow those by Wei and Zunger [31]: (1) the magnitude of the band gap pressure coefficient $|\alpha_p|$ increases with periodically increasing anion atomic number due to the rapid decrease in the bulk modulus B . For example, $\alpha_p = -0.34$ meV/kB for AgCl and -0.75 meV/kB for AgBr; 4.14 meV/kB for CdS and 8.90 meV/kB for CdTe; 3.97 meV/kB for GaN and 11.67 meV/kB for GaAs; -12.18 meV/kB for PdBr₂ and -17.10 meV/kB for PdI₂; 5.94 meV/kB for ZnSe and 9.93 meV/kB for ZnTe. The decrease in the orbital energy difference $\mu^c - \mu^a$, as the anion atomic number increases, is partially canceled by an increasing bond length l contributing to the deformation potential α_v . (2) $|\alpha_p|$ decreases with periodically increasing cation atomic number due to the decrease in the deformation potential over the bulk modulus, which is attributed to increasing $\mu^c - \mu^a$ and l . For example, $\alpha_p = 7.58$ meV/kB for ZnSe, 4.45 meV/kB for CdSe, 1.05 meV/kB for FeSe₂, 0.39 meV/kB for RuSe₂, -16.73 meV/kB for GeSe, -6.04 meV/kB for PbSe; -28.46 meV/kB for SiAs₂ and -20.53 for GeAs₂. (3) The first two conclusions fail when the optical transitions change from direct $\Gamma - \Gamma$ to indirect processes due to the typically stronger matrix elements M at Γ point compared with other \mathbf{k} points. For instance, $\Gamma - L$ band gap pressure coefficient of GaP is 3.80 meV/kB, which falls between GaN (3.97 meV/kB) and GaAs (11.67 meV/kB) with $\Gamma - \Gamma$ transitions. Additionally, it is lower than $\alpha_p = 8.46$ meV/kB for InP with a $\Gamma - \Gamma$ direct band gap. (4) Ionic crystals exhibit smaller $|\alpha_v|$ in contrast to covalent ones of similar bond length because of the larger $\mu^c - \mu^a$ and smaller M . For example, $\alpha_v = -2.99$ eV and 0.13 eV for CdTe and BaTe₃ with a similar bond length (3.30 Å), $\alpha_v = 0.54$ eV and 3.23 eV for Na₂AgSb and SiAs₂ with a similar bond length (2.99 Å and 2.98 Å). (5) Molecules with

multiple identical cations or anions display larger $|\alpha_v|$ than those with a single cation or anion, given that the band edge is typically formed by hybridization among identical atomic species. For example, $\alpha_v = 4.56$ eV and 0.45 eV for Te_2I and TeI , $\alpha_v = 2.46$ eV and 2.83 eV for GeAs and GeAs_2 , $\alpha_v = 0.16$ eV and 2.19 eV for CaP and CaP_3 . These intuitive rules can serve as guidelines to rationally discover and design materials with an enhanced band gap pressure coefficient and photostriction.

IV. CONCLUSION

In summary, through first-principles DFT simulations, we showed that simple thermodynamic descriptors, i.e. the band gap pressure and stress coefficients, can be used to accurately predict the intrinsic photostrictive coefficients in isotropic and anisotropic semiconductors. Motivated by this finding, we conducted a high-throughput search for promising photostrictive materials by screening over 4770 semiconducting materials with band gaps ranging from 0 to 2 eV, where we identified strong photostriction in PtS_2 and Te_2I that is at least one order of magnitude higher than that in MAPbI_3 . Furthermore, we analyzed in detail the impact of bulk modulus and deformation potentials on determining the band gap pressure coefficient and the photostriction. We found that relatively low bulk moduli, which decrease with increasing bond lengths, are an important factor, agreeing with the physical intuition that materials with lower bulk moduli are more susceptible to distortion under external influences. For materials with similar bulk moduli, a simplified LCAO model was adopted for the analysis of the deformation potentials. We concluded that small orbital energy differences $\mu^c - \mu^a$ and large matrix elements M at the band edges are favorable for achieving a large band gap pressure coefficient and a strong photostriction. Our work provides guidelines for understanding intrinsic photostrictive behaviors from the point of view of band gap changes with external pressure and stress and predicts new promising photostrictive materials for optomechanical applications.

ACKNOWLEDGMENTS

This work is based on research supported by the U.S. Office of Naval Research under the award number N00014-22-1-2262. Y.C. also acknowledges the support from the Grad-

Table III. The band gap pressure coefficient and the band gap volume coefficient of selected semiconductors.

	Band Gap Pressure Coefficient, (meV/kB)	Band Gap Volume Coefficient, (eV)
AgCl	-0.34	0.16
AgBr	-0.75	0.33
BaTe ₃	-0.51	0.13
CaP	-0.29	0.16
CaP ₃	-4.17	0.16
CdS	4.14	-2.24
CdSe	4.45	-2.23
CdTe	8.90	-2.99
FeSe ₂	1.05	-1.19
GaN	3.97	-6.75
GaP	3.80	-3.03
GaAs	11.67	-7.30
GeAs	-16.75	2.46
GeAs ₂	-20.53	2.83
GeSe	-16.73	3.87
InP	8.46	-5.45
Na ₂ AgSb	-1.89	0.54
PdBr ₂	-12.18	0.83
PdI ₂	-17.10	1.63
PbSe	-6.04	3.03
RuSe ₂	0.39	-0.56
SiAs ₂	-28.46	3.23
TeI	-5.83	0.45
Te ₂ I	-48.53	4.56
ZnSe	5.94	-3.40
ZnTe	9.93	-4.21

uate Traineeship Program of the NSF Quantum Foundry via the Q-AMASE-i program under award number DMR-1906325 at the University of California, Santa Barbara (UCSB). This work used Stampede2 at Texas Advanced Computing Center (TACC) and Expanse at San Diego Supercomputer Center (SDSC) through allocation MAT200011 from the Advanced Cyberinfrastructure Coordination Ecosystem: Services & Support (ACCESS) program, which is supported by National Science Foundation grants 2138259, 2138286, 2138307, 2137603, and 2138296. Use was also made of computational facilities purchased with funds from the National Science Foundation (CNS-1725797) and administered by the Center for Scientific Computing (CSC). The CSC is supported by the California NanoSystems Institute and the Materials Research Science and Engineering Center (MRSEC; NSF DMR 2308708) at UCSB.

-
- [1] P. Poosanaas, K. Tonooka, and K. Uchino, Photostrictive actuators, *Mechatronics* **10**, 467 (2000).
 - [2] C. Chen and Z. Yi, Photostrictive effect: characterization techniques, materials, and applications, *Advanced Functional Materials* **31**, 2010706 (2021).
 - [3] M. Liparo, J.-P. Jay, M. Dubreuil, G. Simon, A. Fessant, W. Jahjah, Y. Le Grand, C. Shepard, A. R. Prinsloo, V. Vlaminc, *et al.*, Static and dynamic magnetization control of extrinsic multiferroics by the converse magneto-photostrictive effect, *Communications Physics* **6**, 356 (2023).
 - [4] T. Lafont, L. Gimeno, J. Delamare, G. Lebedev, D. Zakharov, B. Viala, O. Cugat, N. Galopin, L. Garbuio, and O. Geoffroy, Magnetostrictive–piezoelectric composite structures for energy harvesting, *Journal of Micromechanics and Microengineering* **22**, 094009 (2012).
 - [5] W. Gauster and D. Habing, Electronic volume effect in silicon, *Physical Review Letters* **18**, 1058 (1967).
 - [6] T. Figielski, Photostriction effect in germanium, *Physica Status Solidi (b)* **1**, 306 (1961).
 - [7] J. North and R. Buschert, Length changes in electron-irradiated n-and p-type germanium, *Physical Review* **143**, 609 (1966).
 - [8] J. Lagowski and H. C. Gatos, Photomechanical vibration of thin crystals of polar semiconductors, *Surface Science* **45**, 353 (1974).

- [9] J. Lagowski and H. Gatos, Photomechanical effect in noncentrosymmetric semiconductors-CdS, *Applied Physics Letters* **20**, 14 (1972).
- [10] D. Schick, M. Herzog, H. Wen, P. Chen, C. Adamo, P. Gaal, D. G. Schlom, P. G. Evans, Y. Li, and M. Bargheer, Localized excited charge carriers generate ultrafast inhomogeneous strain in the multiferroic BiFeO₃, *Physical Review Letters* **112**, 097602 (2014).
- [11] C. Paillard, B. Xu, B. Dkhil, G. Geneste, and L. Bellaiche, Photostriction in ferroelectrics from density functional theory, *Physical Review Letters* **116**, 247401 (2016).
- [12] A. Dogan, P. Poosanaas, I. R. Abothu, S. Komarneni, and K. Uchino, Nanocomposite PLZT ceramic materials in comparison with other processing technique for photostrictive application, *Journal of the Ceramic Society of Japan* **109**, 493 (2001).
- [13] B. Kundys, Photostrictive materials, *Applied Physics Reviews* **2** (2015).
- [14] Y. Kuzukawa, A. Ganjoo, and K. Shimakawa, Photoinduced structural changes in obliquely deposited As- and Ge-based amorphous chalcogenides: correlation between changes in thickness and band gap, *Journal of Non-crystalline Solids* **227**, 715 (1998).
- [15] H. Finkelmann, E. Nishikawa, G. Pereira, and M. Warner, A new opto-mechanical effect in solids, *Physical Review Letters* **87**, 015501 (2001).
- [16] Y. Zhou, L. You, S. Wang, Z. Ku, H. Fan, D. Schmidt, A. Rusydi, L. Chang, L. Wang, P. Ren, *et al.*, Giant photostriction in organic-inorganic lead halide perovskites, *Nature Communications* **7**, 11193 (2016).
- [17] X. Lv, S. Dong, X. Huang, B. Cao, S. Zeng, Y. Wang, T. Wu, L. Chen, J. Wang, G. Yuan, *et al.*, Giant bulk photostriction and accurate photomechanical actuation in hybrid perovskites, *Advanced Optical Materials* **9**, 2100837 (2021).
- [18] T.-C. Wei, H.-P. Wang, H.-J. Liu, D.-S. Tsai, J.-J. Ke, C.-L. Wu, Y.-P. Yin, Q. Zhan, G.-R. Lin, Y.-H. Chu, *et al.*, Photostriction of strontium ruthenate, *Nature Communications* **8**, 15018 (2017).
- [19] B. Kaduk, T. Kowalczyk, and T. Van Voorhis, Constrained density functional theory, *Chemical Reviews* **112**, 321 (2012).
- [20] C. Paillard, S. Prosandeev, and L. Bellaiche, Ab initio approach to photostriction in classical ferroelectric materials, *Physical Review B* **96**, 045205 (2017).
- [21] B. Peng, D. Bennett, I. Bravić, and B. Monserrat, Tunable photostriction of halide perovskites through energy dependent photoexcitation, *Physical Review Materials* **6**, L082401 (2022).

- [22] R. Dronskowski and P. E. Bloechl, Crystal orbital Hamilton populations (COHP): Energy-resolved visualization of chemical bonding in solids based on density-functional calculations, *The Journal of Physical Chemistry* **97**, 8617 (1993).
- [23] V. L. Deringer, A. L. Tchougréeff, and R. Dronskowski, Crystal orbital Hamilton population (COHP) analysis as projected from plane-wave basis sets, *J. Phys. Chem. A* **115**, 5461 (2011).
- [24] P. Würfel and U. Würfel, *Physics of solar cells: from basic principles to advanced concepts* (John Wiley & Sons, 2016).
- [25] G. Kresse and J. Furthmüller, Efficiency of ab-initio total energy calculations for metals and semiconductors using a plane-wave basis set, *Computational Materials Science* **6**, 15 (1996).
- [26] G. Kresse and J. Furthmüller, Efficient iterative schemes for ab initio total-energy calculations using a plane-wave basis set, *Physical Review B* **54**, 11169 (1996).
- [27] P. E. Blochl, Projector augmented-wave method, *Physical Review B* **50**, 17953 (1994).
- [28] J. P. Perdew, K. Burke, and M. Ernzerhof, Generalized gradient approximation made simple, *Physical Review Letters* **77**, 3865 (1996).
- [29] A. Jain, S. P. Ong, G. Hautier, W. Chen, W. D. Richards, S. Dacek, S. Cholia, D. Gunter, D. Skinner, G. Ceder, *et al.*, Commentary: The materials project: A materials genome approach to accelerating materials innovation, *APL Materials* **1** (2013).
- [30] B. Welber, M. Cardona, C. Kim, and S. Rodriguez, Dependence of the direct energy gap of GaAs on hydrostatic pressure, *Physical Review B* **12**, 5729 (1975).
- [31] S.-H. Wei and A. Zunger, Predicted band-gap pressure coefficients of all diamond and zinc-blende semiconductors: Chemical trends, *Physical Review B* **60**, 5404 (1999).
- [32] R. Dornhaus, G. Nimtz, and B. Schlicht, *Narrow-gap semiconductors*, Vol. 98 (Springer, 2006).
- [33] S.-H. Wei and A. Zunger, Electronic and structural anomalies in lead chalcogenides, *Physical Review B* **55**, 13605 (1997).
- [34] J. Yuan, Y. Chen, and B. Liao, Lattice dynamics and thermal transport in semiconductors with anti-bonding valence bands, *Journal of the American Chemical Society* **145**, 18506 (2023).
- [35] P. Cheng, N. Shulumba, and A. J. Minnich, Thermal transport and phonon focusing in complex molecular crystals: Ab initio study of polythiophene, *Physical Review B* **100**, 094306 (2019).
- [36] Y. Wang, X. Lu, W. Yang, T. Wen, L. Yang, X. Ren, L. Wang, Z. Lin, and Y. Zhao, Pressure-induced phase transformation, reversible amorphization, and anomalous visible light response in organolead bromide perovskite, *Journal of the American Chemical Society* **137**,

- 11144 (2015).
- [37] A. Bagri, A. Jana, G. Panchal, D. M. Phase, and R. J. Choudhary, Amalgamation of photostriction, photodomain, and photopolarization effects in BaTiO₃ and its electronic origin, *ACS Applied Electronic Materials* **4**, 4438 (2022).
- [38] S. Soled, A. Wold, and O. Gorochoy, Crystal growth and characterization of several platinum sulfoselenides, *Materials Research Bulletin* **11**, 927 (1976).
- [39] G. Guo and W. Liang, The electronic structures of platinum dichalcogenides: Pts₂, ptse₂ and ptte₂, *Journal of Physics C: Solid State Physics* **19**, 995 (1986).
- [40] C. P. Cullen, C. Ó. Coileáin, J. B. McManus, O. Hartwig, D. McCloskey, G. S. Duesberg, and N. McEvoy, Synthesis and characterisation of thin-film platinum disulfide and platinum sulfide, *Nanoscale* **13**, 7403 (2021).
- [41] E. Anastassakis, J. Raptis, and W. Richter, Raman and infrared spectra of tellurium sub-bromide (te₂br), *Physica Status Solidi (b)* **130**, 161 (1985).
- [42] R. Kniep, D. Mootz, and A. Rabenau, Zur kenntnis der subhalogenide des tellurs, *Zeitschrift für anorganische und allgemeine Chemie* **422**, 17 (1976).
- [43] W. A. Harrison, *Electronic structure and the properties of solids: the physics of the chemical bond* (Courier Corporation, 2012).

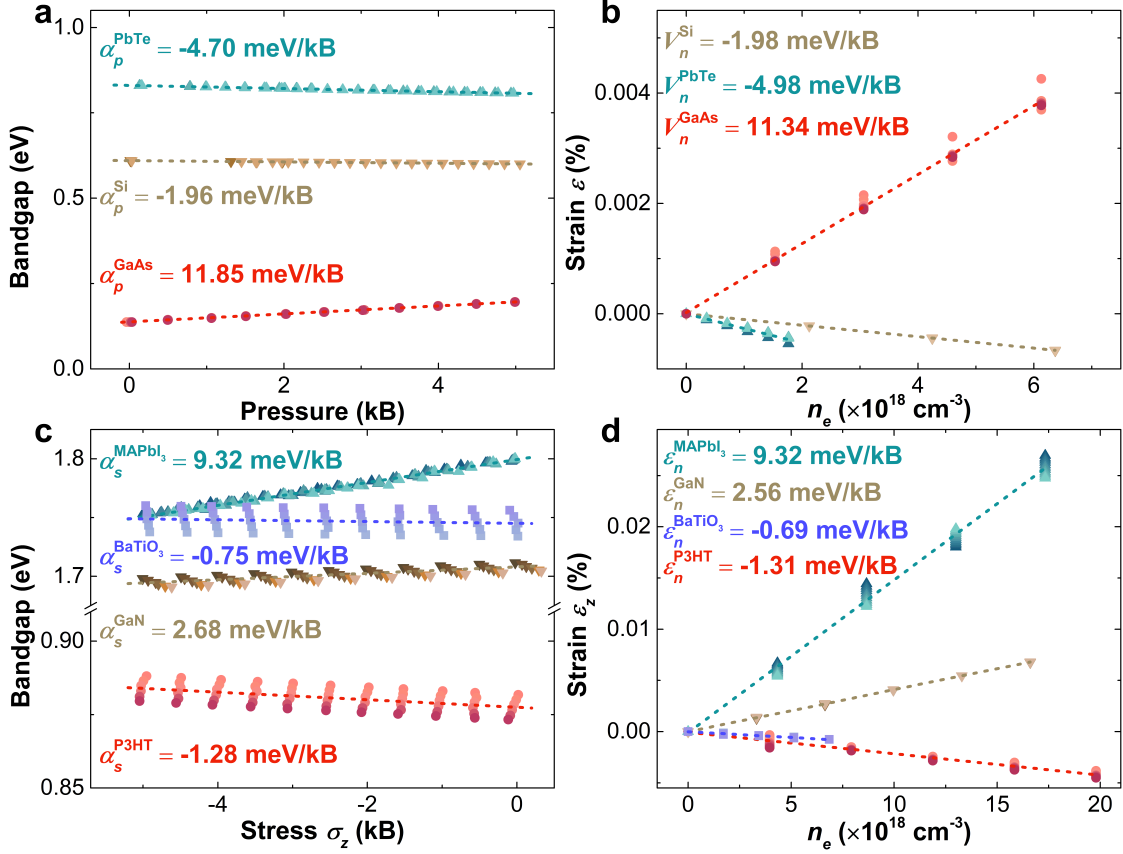


Figure 1. **Relationship between the photostriction coefficients and the band gap pressure/stress coefficients.** **a.** Band gap changes with hydrostatic pressure at different excited electron densities corresponding to the range shown in **b** (represented by different shades of the marker color) for isotropic materials (Si, PbTe, and GaAs). Band gap pressure coefficient fittings (averaged over different excited electron densities) are denoted by dashed lines. **b.** Photo-induced strain change with excited electron densities at different hydrostatic pressures corresponding to the range shown in **a** (represented by different shades of the marker color) for isotropic materials. Volumetric photostriction coefficient fittings (averaged at different hydrostatic pressures) are denoted by dashed lines. **c.** Band gap changes with stress along the out-of-plane (z) direction with different excited electron densities for anisotropic materials (GaN, MAPbI₃, PT, and BaTiO₃). **d.** Photo-induced strain along the out-of-plane (z) direction as a function of excited electron densities for anisotropic materials.

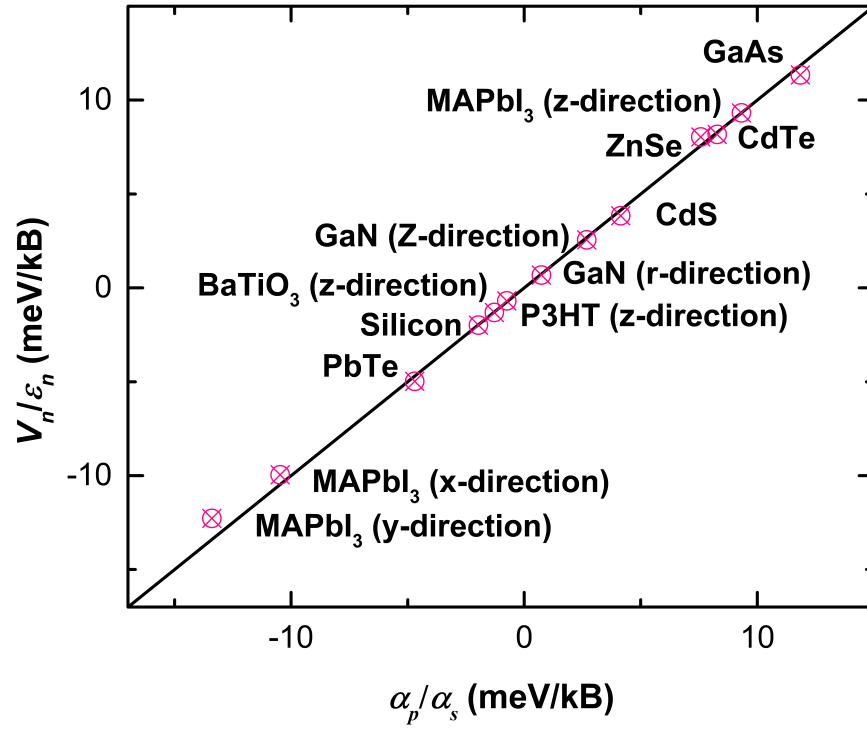


Figure 2. Comparison between the photostriction coefficients (V_n/ϵ_n) and the band gap pressure (stress) coefficients (α_p/α_s) across different materials.

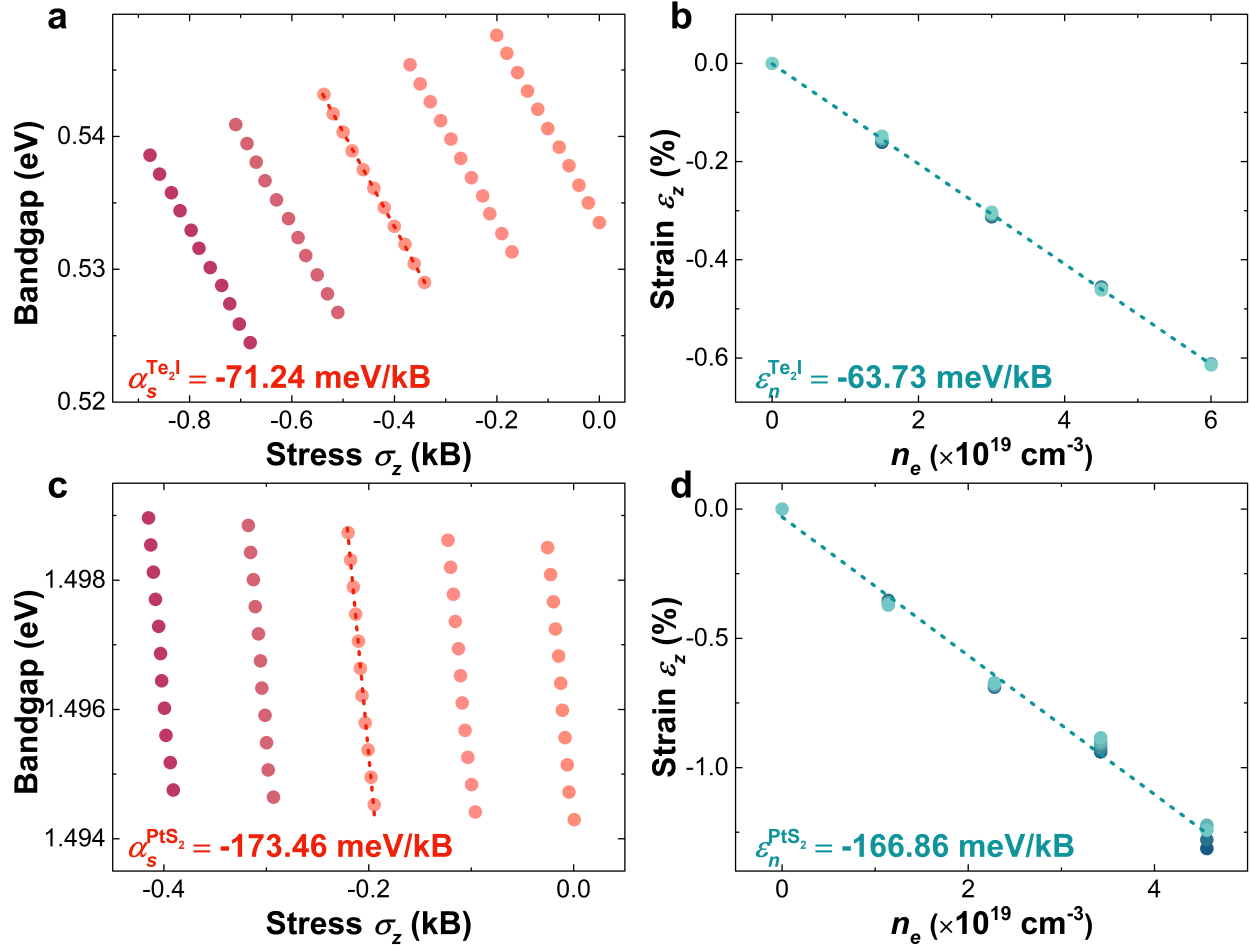


Figure 3. **Photostriction and band gap stress coefficients in Te₂I and PtS₂.** **a.** Te₂I band gap changes with stress along the out-of-plane (z) direction with different excited electron densities corresponding to the range shown in **b** (represented by different shades of the marker color). The band gap stress coefficient averaged over different excited electron densities (dashed line) is fitted as -71.24 meV/kB. **b.** Te₂I strain change along the out-of-plane direction as a function of excited electron densities at different stress corresponding to the range in **a** (represented by different shades of the marker color). The photostriction coefficient averaged over different stress (dashed line) is fitted as -63.73 meV/kB. Similar plots for PtS₂ are presented in **c** and **d**.

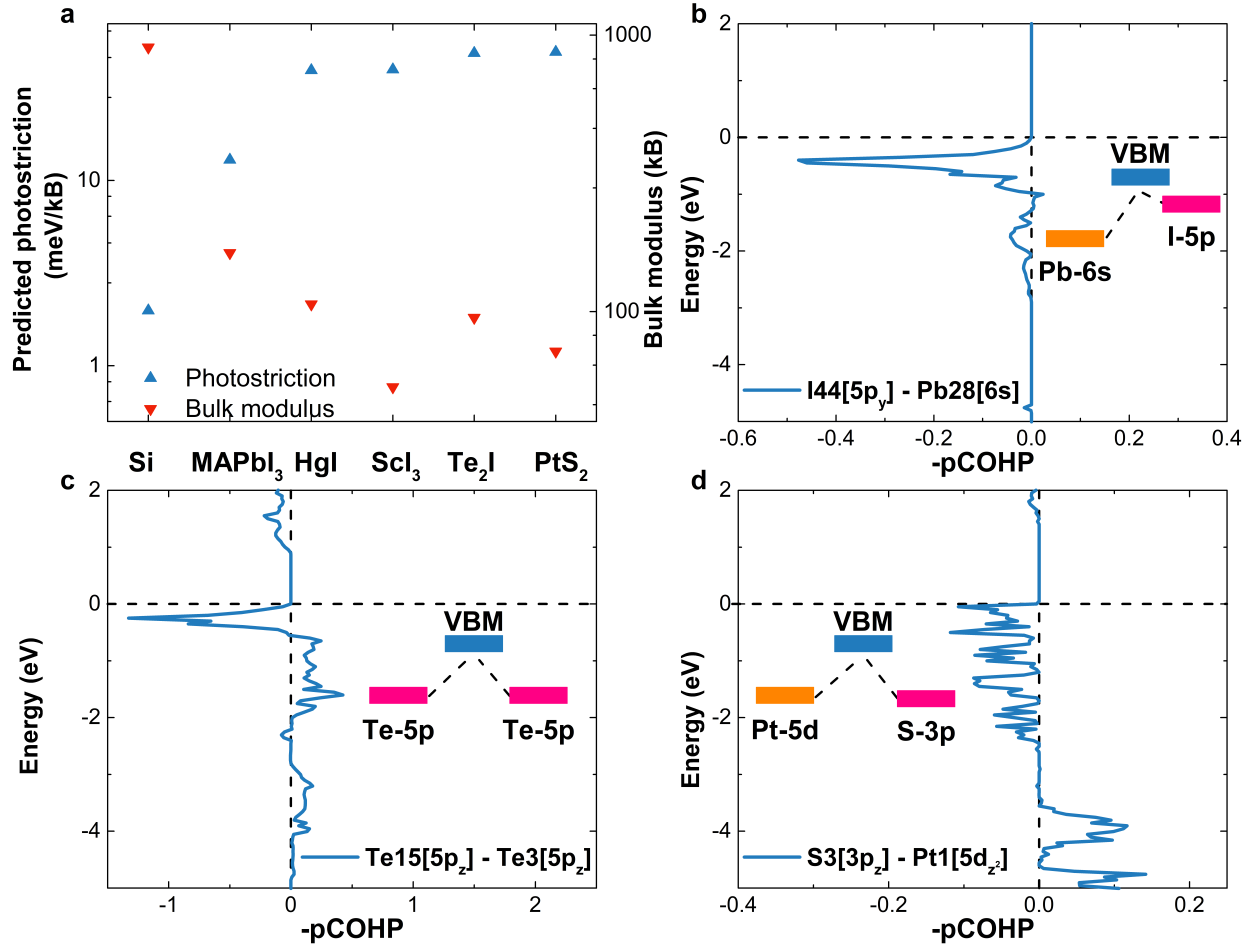


Figure 4. **Analysis of factors impacting photostriction.** a. Predicted photostriction and the bulk modulus of Si, MAPbI₃, HgI, ScI₃, Te₂I, and PtS₂. b-d. COHP diagrams of MAPbI₃, Te₂I, and PtS₂, with insets highlighting strongest anti-bonding interactions between orbitals near VBM.

Supplementary Information: High-Throughput Search for Photostrictive Materials based on a Thermodynamic Descriptor

Zeyu Xiang,^{1,*} Yubi Chen,^{1,2,*} Yujie Quan,¹ and Bolin Liao^{1,†}

¹*Department of Mechanical Engineering,*

University of California, Santa Barbara, CA 93106, USA

²*Department of Physics, University of California, Santa Barbara, CA 93106, USA*

(Dated: August 21, 2024)

arXiv:2408.11044v1 [cond-mat.mtrl-sci] 20 Aug 2024

* These authors contributed equally.

† bliao@ucsb.edu

I. LATTICE STRUCTURES AND CRYSTAL ORIENTATIONS

A. GaN, MAPbI₃, PT, and BaTiO₃

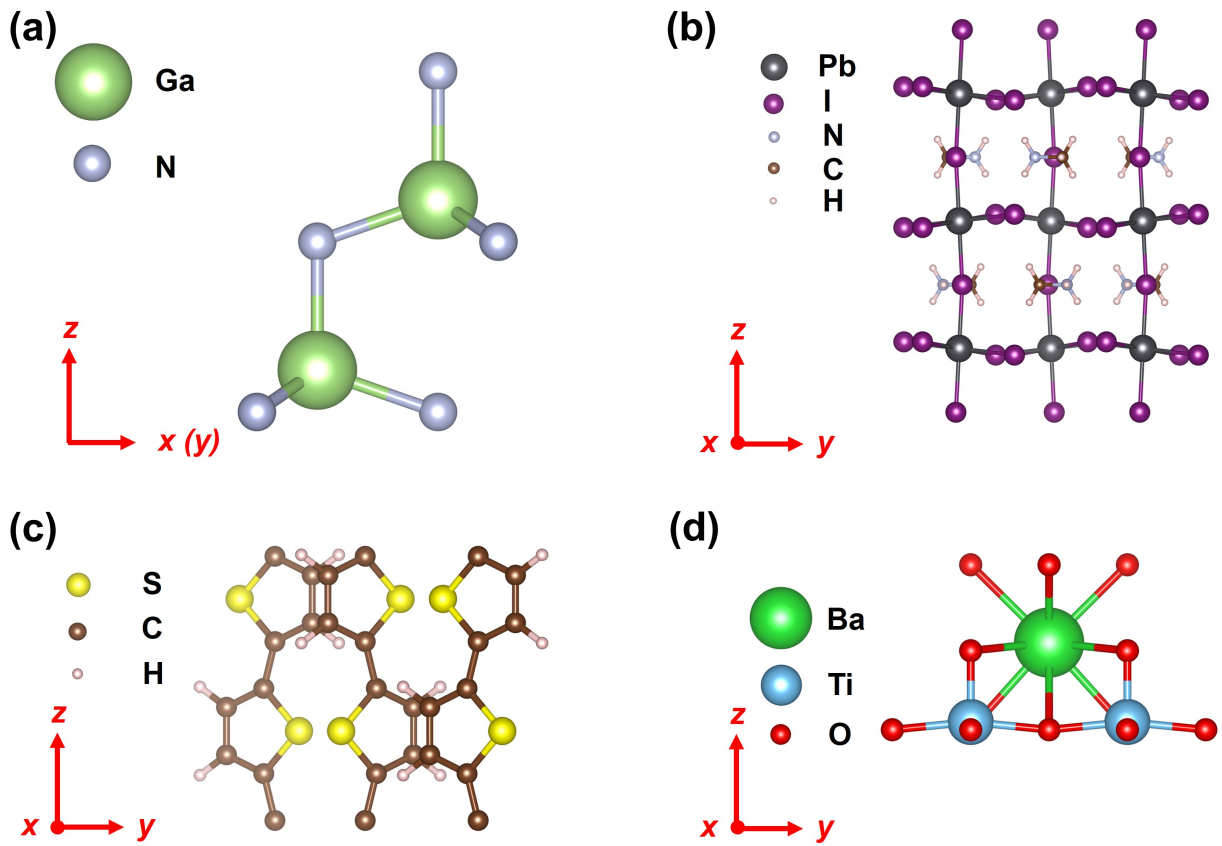


Figure S1. Schematic illustrations of lattice structures and crystal orientations for the unit cell of several anisotropic materials studied in this work. a, GaN. b, MAPbI₃. c, PT. d, BaTiO₃. The x(y) direction refers to the in-plane direction. The z direction refers to the out-of-plane direction.

B. PtS_2 and Te_2I

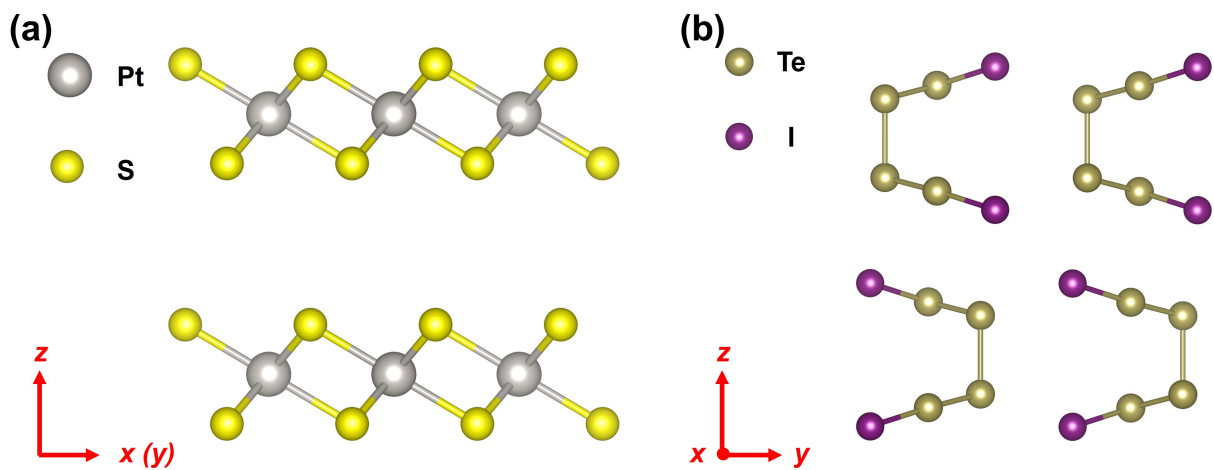


Figure S2. Schematic illustrations of lattice structures and crystal orientations for the unit cells of PtS_2 and Te_2I . **a**, PtS_2 . **b**, Te_2I . The z direction refers to the out-of-plane direction.

II. VERIFICATION OF THERMODYNAMIC RELATION FOR TYPICAL MATERIALS

A. Isotropic materials including CdS, CdTe, GaAs, and ZnSe

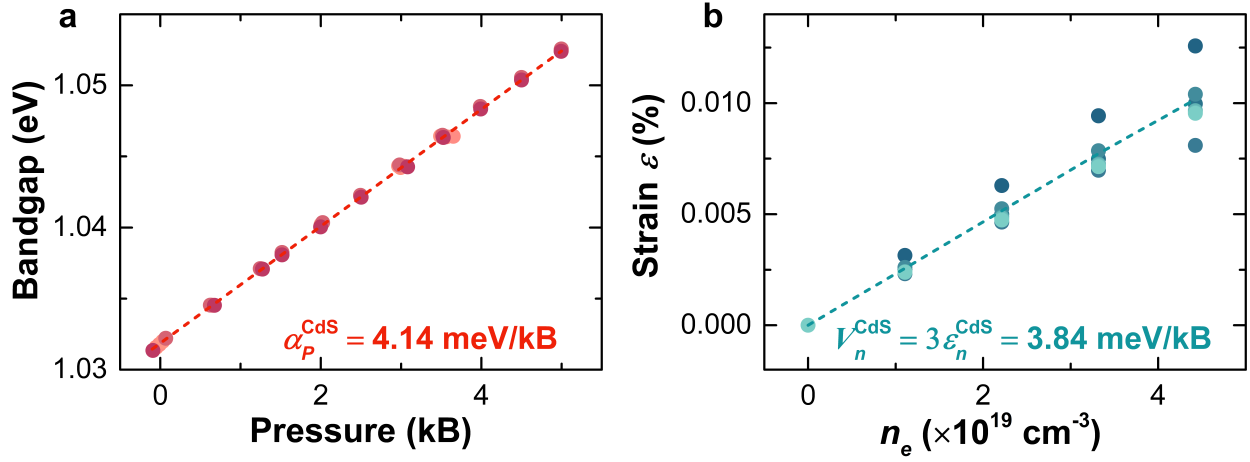


Figure S3. **a**, CdS band gap change with hydrostatic pressure under different excited electron densities. Band gap pressure coefficient (dashed line) is fitted as 4.14 meV/kB. **b**, CdS strain change with excited electron densities at different hydrostatic pressures. Photostriction (dashed line) is fitted as 3.84 meV/kB.

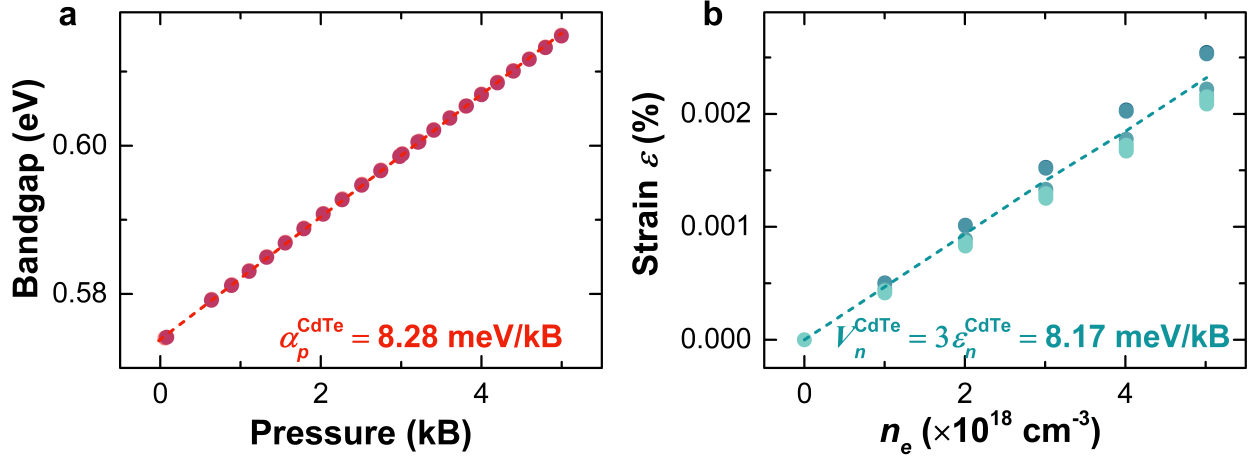


Figure S4. **a**, CdTe band gap change with hydrostatic pressure under different excited electron densities. Band gap pressure coefficient (dashed line) is fitted as 8.28 meV/kB. **b**, CdTe strain change with excited electron densities at different hydrostatic pressures. Photostriction (dashed line) is fitted as 8.17 meV/kB.

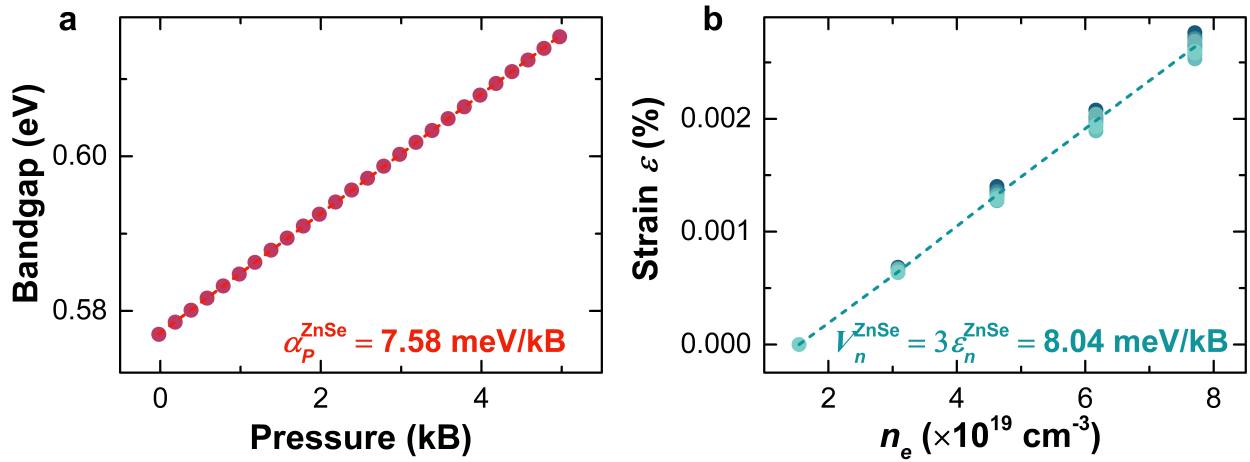


Figure S5. **a**, ZnSe band gap change with hydrostatic pressure under different excited electron densities. Band gap pressure coefficient (dashed line) is fitted as 7.58 meV/kB. **b**, ZnSe strain change with excited electron densities at different hydrostatic pressures. Photostriction (dashed line) is fitted as 8.04 meV/kB.

B. In-plane (r) directions of anisotropic material GaN

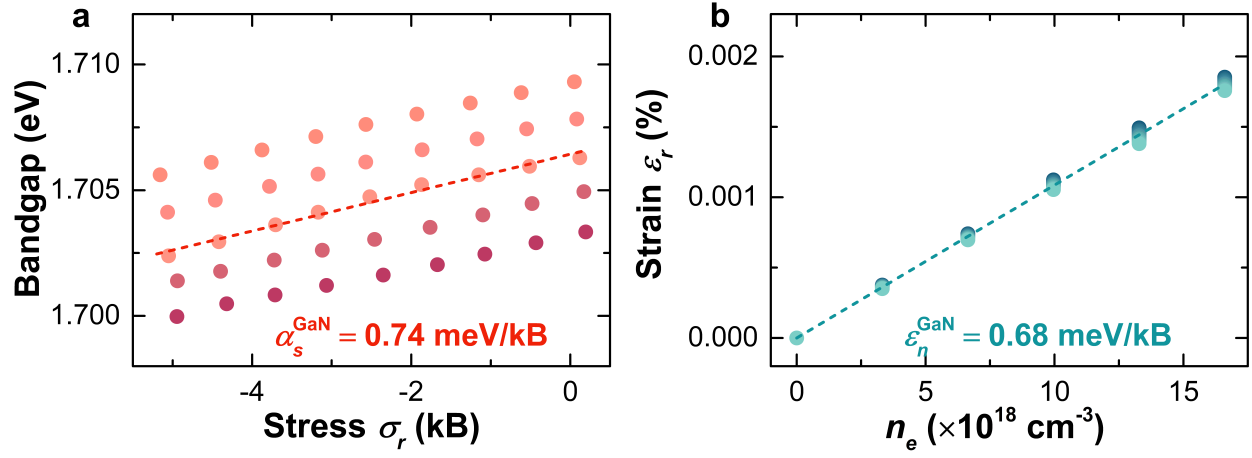


Figure S6. **a**, GaN band gap change with stress along in-plane (r) direction (in-plane symmetry) under different excited electron densities. Band gap stress coefficient (dashed line) is fitted as 0.74 meV/kB. **b**, GaN strain change along r direction with excited electron densities at different pressures. Photostriction (dashed line) is fitted as 0.68 meV/kB.

C. In-plane (x and y) directions of anisotropic material MAPbI₃

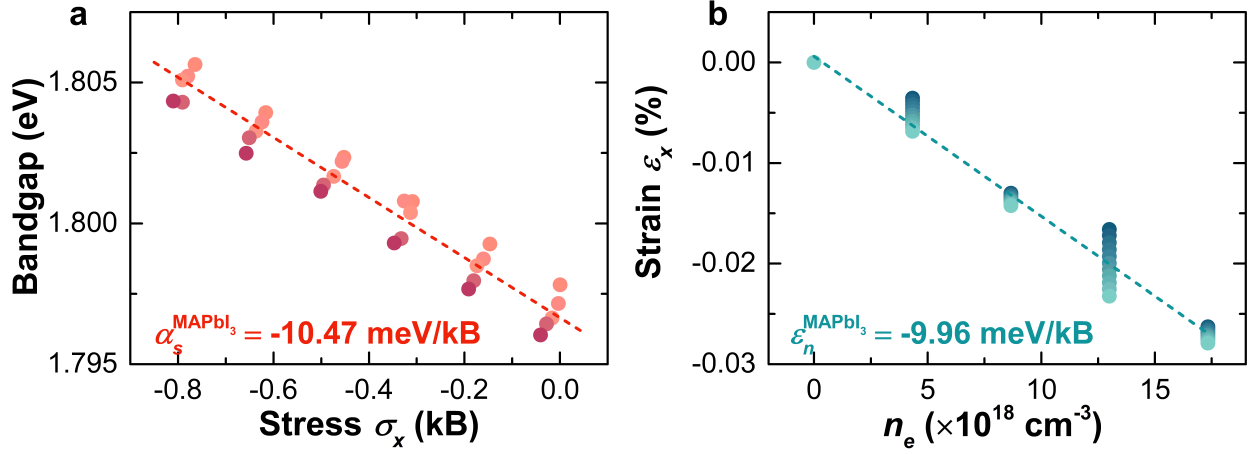


Figure S7. **a**, MAPbI₃ band gap change with stress along in-plane (x) direction under different excited electron densities. Band gap stress coefficient (dashed line) is fitted as -10.47 meV/kB. **b**, MAPbI₃ strain change along x direction with excited electron densities at different pressures. Photostriction (dashed line) is fitted as -9.96 meV/kB.

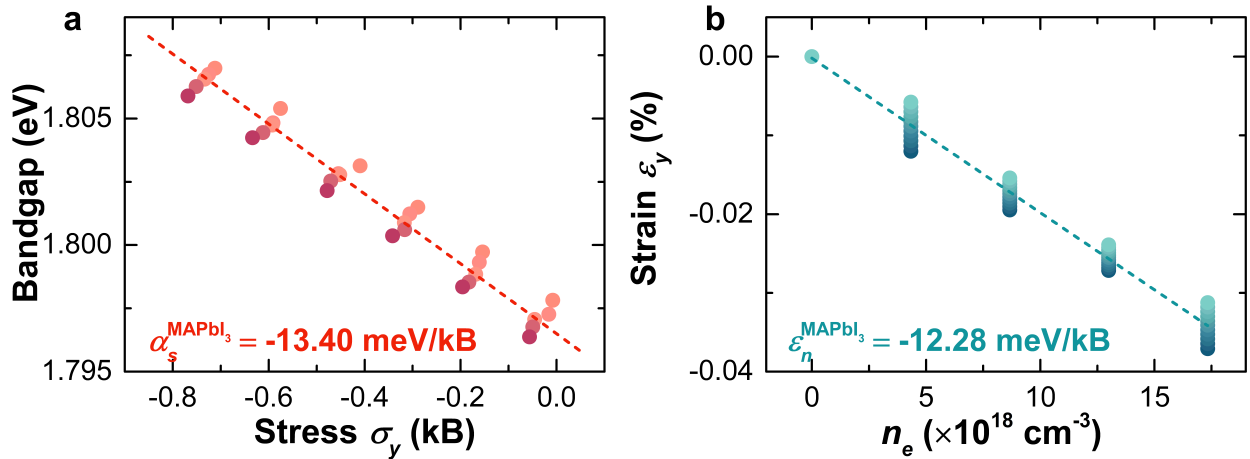


Figure S8. **a**, MAPbI₃ band gap change with stress along in-plane (y) direction under different excited electron densities. Band gap stress coefficient (dashed line) is fitted as -13.40 meV/kB. **b**, MAPbI₃ strain change along y direction with excited electron densities at different pressures. Photostriction (dashed line) is fitted as -12.28 meV/kB.

III. ANALYSIS OF BAND GAP PRESSURE COEFFICIENTS FOR DISCOVERED MATERIALS IN HIGH-THROUGHPUT SEARCH

A. Relationship between band gap pressure coefficient and bulk modulus

A decreasing trend in amplitude of band gap pressure coefficient with bulk modulus is observed after analyzing 4770 materials. As presented in Fig. S9a, the decreasing trend becomes significant after segmenting the entire region based on the magnitude of α_V . Fig. S9b shows that the bulk modulus decreases with increasing bond length. Taking this into consideration, it is reasonable to conclude photostriction (band gap pressure coefficient) generally shows an upward trend with increasing bond length.

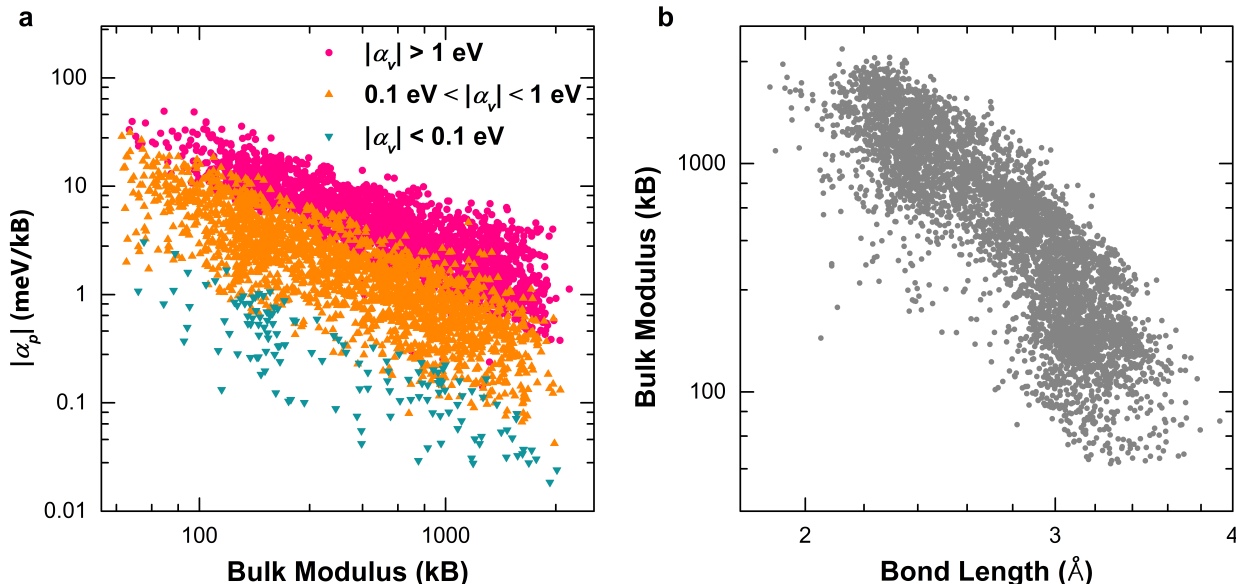


Figure S9. a, Magnitude of band gap pressure coefficient with bulk modulus, segmented into three regions by the magnitude of α_v . b, Change of bulk modulus with averaged bond length.

B. Candidate materials with large band gap pressure coefficient

The following table contains the band gap pressure coefficient of top 500 stable materials with PBE-calculated band gap between 0 and 2 eV from the Materials Project[1]. Band gap pressure coefficients are determined by linear regression of the band gap change with hydrostatic pressure (2 kB, 6 kB, and 10 kB). The list is sorted by the amplitude of the

band gap pressure coefficient.

Table S1: Top 500 photostrictive materials (with the Materials Project ID number).

Material	band gap Pressure Coefficient (meV/kB)
PtS ₂ -mp762	-49.2331
Te ₂ I-mp27655	-48.5868
ScI ₃ -mp1186991	-39.6388
HgI-mp22859	-39.282
Te ₂ Br-mp27648	-38.7564
AsS-mp542810	-38.3489
PdSe ₂ -mp2418	-35.824
WS ₂ -mp224	-33.7557
PdS ₂ -mp13682	-33.5788
PAuS ₄ -mp30938	-33.2683
WSe ₂ -mp1821	-33.0542
SiAs-mp1863	-32.8593
Cs ₂ Se ₅ -mp541055	-32.3042
AuSe-mp2793	-31.6278
PI ₂ -mp29443	-31.2949
InS-mp19795	-31.1798
AsSe-mp542570	-30.8151
MoSe ₂ -mp1634	-30.1618
InSe-mp20485	-29.8206
TlBr ₂ -mp27398	-29.8043
CsSbS ₆ -mp28701	-29.2265
Rb ₂ Se ₅ -mp620372	-28.9617
Ga ₂ PdI ₈ -mp30946	-28.9043
Se-mp570481	-28.8784
Cs ₂ TlAsI ₆ -mp1112544	-28.5609
SiAs ₂ -mp978553	-28.4574

Material	band gap Pressure Coefficient (meV/kB)
SnGeS ₃ -mp5045	-28.0819
Cs ₂ S ₅ -mp1193140	-28.0509
Rb ₂ TlSbCl ₆ -mp1114002	-27.8811
CsK ₂ Sb-mp581024	27.6284
CdP ₁₄ Pb-mp1214259	-27.1008
P ₃ Se ₄ I-mp28393	-26.7091
Rb ₂ S ₅ -mp16911	-26.6534
GeP-mp1095275	-26.6284
P-mp568348	-26.1563
Tl ₃ Cd ₂ I ₇ -mp28432	-26.1179
SbI ₃ Cl ₈ -mp23536	-25.7183
TiI ₄ -mp541013	-25.615
NbI ₅ -mp569578	-25.2136
CsGeI ₃ -mp28377	-25.0838
SbI ₃ (BrCl ₃) ₂ -mp570962	-25.0286
Te ₂ Mo-mp602	-24.7159
Pd(Se ₃ Br) ₂ -mp2422143	-24.5998
CsK ₂ Bi-mp863759	23.9411
As ₂ Se ₃ -mp909	-23.8915
InI ₂ -mp29312	-23.6691
HI ₃ -mp1184859	-23.4911
RbAu ₃ Se ₂ -mp9385	-23.4292
CdSnP ₁₄ -mp1199087	-23.2282
Nb ₂ Se ₁₇ Cl ₁₂ -mp573340	-22.916
ThTe ₃ -mp1025522	-22.7052
K ₂ Se ₅ -mp18609	-22.5947
SiP ₂ -mp9996	-22.0264
BP(IBr) ₃ -mp567433	-21.9507
InBr-mp22870	-21.8804

Material	band gap Pressure Coefficient (meV/kB)
Rb ₃ Au ₃ Cl ₈ -mp27301	-21.5006
K ₂ S ₅ -mp17146	-21.4127
BiTeCl-mp28944	-21.2176
CsTaI ₆ -mp606510	-21.0869
CsInBr ₃ -mp1112338	-20.9722
GeI ₄ -mp23266	-20.9475
P ₃ BrCl ₁₄ -mp29033	20.702
Tl ₃ SbS ₄ -mp8378	-20.6668
MoS ₂ -mp1434	-20.6525
GeAs ₂ -mp17524	-20.5343
K ₇ TaAs ₄ -mp18073	20.4017
Al ₂ Te ₃ -mp29502	-20.3344
GaSe-mp568263	-20.3016
Bi ₉ Ir ₂ I ₃ -mp680182	-20.2553
KBaPSe ₄ -mp18156	-20.0827
TlSb ₃ S ₅ -mp27515	-19.5847
HfSnS ₃ -mp8725	-19.3201
PICl ₆ -mp27824	19.1764
InI-mp23202	-19.1215
TlI ₃ -mp28329	-18.9936
HgI ₂ -mp23192	-18.9549
ICl ₃ -mp27729	-18.9476
C(Se ₂ Br) ₂ -mp28131	-18.9361
PBr ₅ -mp22874	18.9155
Cs ₆ InAs ₃ -mp22506	18.8649
RbInCl ₃ -mp1114001	-18.8596
RbAuBr ₃ -mp27300	-18.8048
Tl ₅ Se ₂ Cl-mp28920	-18.7913
TlCuPS ₃ -mp1190539	-18.7649

Material	band gap Pressure Coefficient (meV/kB)
TlSnPS ₄ -mp6057	-18.7399
Hg ₃ TeBr ₄ -mp29097	-18.7319
TlAuCl ₄ -mp28368	-18.6798
PBr ₇ -mp647343	18.6185
Cs ₂ Te-mp573763	18.43
Tl ₃ BSe ₃ -mp28490	-18.4141
Na ₃ AlAs ₂ -mp8543	18.3579
K ₂ NaAlP ₂ -mp9068	18.3427
Cs ₃ Na ₂ SnP ₃ -mp17707	18.2693
KNaTe-mp8755	18.2291
Tl ₂ Hg ₃ Se ₄ -mp1105692	-18.1671
GaTeI ₇ -mp29541	-18.1592
Bi ₂ Se ₃ -mp541837	-18.1291
Rb ₂ P ₂ Pt-mp1205641	-17.8567
Rb ₂ As ₂ Pt-mp13445	-17.7568
K ₅ Tl ₃ O-mp555531	17.7068
InTeBr-mp29236	-17.6732
AlHg ₂ SbCl ₄ -mp568001	17.6571
Cs ₂ SnBr ₆ -mp641923	-17.6139
TlSe-mp1836	-17.6069
K ₇ NbAs ₄ -mp18361	17.566
Cs ₃ BAs ₂ -mp573658	17.5432
Rb ₂ SnBr ₆ -mp569028	-17.49
PPdSe-mp3123	-17.4006
K ₂ NaAlAs ₂ -mp9069	17.3567
GePdS ₃ -mp541785	-17.246
PdI ₂ -mp27747	-17.0983
TaTeBr ₉ -mp29716	-17.0979
Tl ₂ Sn ₂ S ₃ -mp28011	-17.0852

Material	band gap Pressure Coefficient (meV/kB)
Ga ₂ Te ₅ -mp2371	-17.0675
GaTe-mp542812	-16.9283
Na ₅ AuSe ₁₂ -mp29198	-16.8263
K ₄ P ₂₁ I-mp31280	-16.8147
CsSn-mp571056	16.7952
GeAs-mp9548	-16.7525
GeSe-mp700	-16.7325
BiI ₅ -mp1214795	-16.6982
K ₂ As ₂ Pt-mp1079513	-16.6839
Sn(BiTe ₂) ₂ -mp38605	-16.6398
Nb ₂ PS ₁₀ -mp648932	-16.632
Rb ₂ Sb ₄ S ₇ -mp561051	-16.6248
NaSbS ₂ -mp5414	-16.6174
CsAuSe ₃ -mp567913	-16.5906
NaSi-mp2402	-16.5655
Hg(SbS ₂) ₄ -mp542596	-16.5612
TiP ₂ (S ₄ Cl) ₂ -mp1203568	-16.542
Cs ₃ As(PSe ₃) ₃ -mp1201199	-16.5088
V ₂ Se ₉ -mp28256	-16.5035
Tl ₂ PdCl ₄ -mp29889	-16.384
GaHg ₂ SbCl ₄ -mp571190	16.3136
Rb ₅ GeP ₃ -mp17978	16.262
K ₂ AgBi-mp27549	16.2294
Tl ₄ PbSe ₃ -mp1195087	-16.18
Na ₃ AlP ₂ -mp5122	16.1209
K ₂ AgAs-mp7642	16.1056
Rb ₃ BA ₂ -mp9718	16.1027
K ₂ NaGaP ₂ -mp9666	15.9499
Si(PbSe ₂) ₂ -mp27532	-15.9444

Material	band gap Pressure Coefficient (meV/kB)
CsHg ₂ Br ₅ -mp619510	-15.8795
Tl ₅ Ag ₃ (PS ₃) ₄ -mp1195546	-15.8093
HgPS ₃ -mp27178	-15.6762
K ₃ Au ₃ Br ₈ -mp1211803	-15.6728
Ag ₂ TeS ₃ -mp29163	-15.6409
HgP ₁₄ Pb-mp22574	-15.6346
Ta ₂ Se ₁₇ Br ₁₂ -mp541758	-15.6219
Rb ₂ PtI ₆ -mp28110	-15.5877
AlTlSe ₂ -mp863762	-15.5499
As ₂ S ₃ -mp1189572	-15.519
TlAsSe ₂ -mp30236	-15.4383
Tb ₂ Te ₃ -mp1105684	-15.3691
InBi ₂ S ₄ Cl-mp559521	-15.3461
SbAs ₂ Cl ₁₃ -mp27786	15.3279
Tl ₂ TeI ₆ -mp31077	-15.3009
Cs ₂ Se-mp1011695	15.2859
CuTe ₂ Cl-mp30971	-15.2785
K ₁₀ NbInAs ₆ -mp1224638	15.2746
ThSe ₃ -mp1079673	-15.2388
AuCl ₂ -mp541656	-15.2299
Tm ₂ Te ₃ -mp1188133	-15.2129
AuCl ₃ -mp27647	-15.0595
Er ₂ Te ₃ -mp14643	-14.989
PdSCl-mp560901	-14.9753
Rb ₃ BP ₂ -mp9720	14.9588
ICl-mp567998	-14.9296
K ₃ Sb ₂ Au ₃ -mp9273	-14.9144
Cs ₅ Tc ₆ S ₈ Br ₇ -mp1182756	-14.9134
Rb ₂ SbAuS ₄ -mp556894	-14.9117

Material	band gap Pressure Coefficient (meV/kB)
KS ₃ -mp1196514	-14.9102
Rb ₄ P ₂₁ I-mp31279	-14.907
Tl ₃ AsS ₄ -mp5704	-14.8805
Rb ₇ NbAs ₄ -mp18440	14.8642
Ho ₂ Te ₃ -mp1189209	-14.8402
SnHg ₆ (As ₂ Br ₃) ₂ -mp567185	14.8243
Cs ₂ AgAuCl ₆ -mp567776	-14.8079
Tl ₃ AsSe ₃ -mp7684	-14.784
Rb ₇ NaGe ₈ -mp14407	14.7421
Rb ₅ SiAs ₃ -mp17490	14.717
RbCaAs-mp9845	14.7149
Sn(S ₄ I) ₄ -mp557101	-14.6968
RbGaH ₂ -mp974682	14.6531
Lu ₂ Te ₃ -mp1189748	-14.6491
RbGe-mp1888	14.632
K ₃ As(PSe ₃) ₃ -mp1197620	-14.6292
Rb ₂ PbCl ₆ -mp23475	-14.6234
Sn(SbTe ₂) ₂ -mp27947	-14.5844
ZrSnS ₃ -mp17324	-14.5458
K ₂ NaGaAs ₂ -mp9676	14.5454
CsTlBr ₄ -mp573702	-14.532
TlAgAs ₂ PbS ₅ -mp677611	-14.4678
Cs ₂ PbCl ₆ -mp23425	-14.4657
AlSiTe ₃ -mp31220	-14.4188
RbSi-mp1074	14.4099
Cs ₂ NaGaP ₂ -mp1213705	14.4009
CsPSe ₆ -mp1225967	-14.3896
Cs ₃ BrO-mp1205638	14.3249
K ₃ BP ₂ -mp9664	14.3117

Material	band gap Pressure Coefficient (meV/kB)
Y_2Te_3 -mp1189791	-14.2932
$Rb_4TlSbCl_{12}$ -mp1219616	-14.2913
$KSbS_2$ -mp11703	-14.288
Tl_2GeS_3 -mp7277	-14.2671
$InSbS_3$ -mp21365	-14.2472
Rb_7NaSi_8 -mp1202504	14.1719
Pr_3RuBr_3 -mp1209743	-14.1628
Dy_2Te_3 -mp1188427	-14.136
Nb_2Se_9 -mp541106	-14.1082
Cs_2Pt -mp13548	14.1007
MnV_2O_6 -mp2490654	-14.0129
Tb_7RhI_{12} -mp1190279	-13.9526
In_5S_5Cl -mp31263	-13.8979
K_2SnBr_6 -mp574040	-13.8762
Tl_3BS_3 -mp29337	-13.8151
K_4BeP_2 -mp9872	13.7772
La_3RuI_3 -mp29824	-13.7687
Tl_3PSe_4 -mp4160	-13.7308
$La(Tl_3Te_2)_3$ -mp1223306	-13.7124
$ZrHg_3(SBr_3)_2$ -mp1207395	13.7104
$TlSbS_2$ -mp676540	-13.6698
Rb_4SnSb_6 -mp505490	-13.6267
K_3InP_2 -mp20256	13.6214
Li_2TeS_3 -mp558731	-13.6185
$ErTl(PSe_3)_2$ -mp1105213	-13.5431
$RbAg_2(AsSe_2)_3$ -mp570593	-13.5378
$PtCl_2$ -mp23290	-13.5248
$KP_2Au_5S_8$ -mp561218	-13.5236
$Rb_{12}Sn_2As_6O$ -mp1219774	13.5164

Material	band gap Pressure Coefficient (meV/kB)
PdCl ₂ -mp29487	-13.5008
Rb ₂ SnAs ₂ -mp8931	13.4733
Te ₃ (PdBr) ₄ -mp638749	-13.4665
TlGaTe ₂ -mp3785	-13.458
K ₅ Au(IO) ₂ -mp558332	13.4438
InTeI-mp29234	-13.4262
Tl ₅ Se ₂ Br-mp28921	-13.3982
Tl ₄ SnS ₄ -mp5818	-13.341
K ₃ Al ₂ As ₃ -mp28347	13.3196
K ₆ InAs ₃ -mp1226185	13.3089
Rb ₃ TlBr ₆ -mp1114103	13.2897
AlSb ₂ (TeCl ₂) ₂ -mp567743	-13.1588
Er ₇ IrI ₁₂ -mp1105808	-13.1334
Re ₃ Br ₈ Cl-mp1219236	-13.1128
K ₃ Na ₂ SnP ₃ -mp16847	13.1025
KPSe ₆ -mp18625	-13.0885
CuP ₁₀ -mp606644	-13.0816
Na ₅ InTe ₄ -mp28597	-13.072
AgI-mp580941	-13.0687
K ₄ ZnBi ₂ -mp1103566	13.0508
Rb ₃ As ₁₁ -mp542233	-13.0106
RbAuSe-mp9731	12.9983
Rb ₃ ClO-mp755428	12.9871
MoBr ₃ O-mp1221539	-12.9478
Tl ₆ SI ₄ -mp27938	-12.921
Re ₃ Se ₂ Br ₅ -mp1173441	-12.9061
Ba ₆ Sn ₆ Se ₁₃ -mp1196224	-12.8915
Tl ₂ PtCl ₆ -mp27834	-12.8757
PrTlTe ₂ -mp999288	-12.874

Material	band gap Pressure Coefficient (meV/kB)
Ga ₄ Hg ₁₁ (AsBr ₄) ₄ -mp669455	12.8301
TlGeCl ₃ -mp998744	-12.8083
EuI ₂ -mp1102093	-12.7687
KAuCl ₄ -mp27181	-12.7559
TlIn ₄ S ₅ Cl-mp1208155	-12.7485
Nb ₂ Te ₆ I-mp28745	-12.7322
K ₅ P ₂ Au-mp14624	12.7251
Ag ₂ HgI ₄ -mp1229122	-12.7176
Cs ₂ As ₂ Pd-mp8857	-12.6856
Rb ₅ FeO ₄ -mp768830	12.6704
NdTlTe ₂ -mp999319	-12.6586
TeAuI-mp27741	-12.6583
Y ₆ PtI ₁₀ -mp1189258	-12.6408
K ₄ HgP ₂ -mp8753	12.6237
CuTe ₂ Br-mp31036	-12.5825
K ₅ As ₂ Au-mp8683	12.5721
TiTiPS ₅ -mp1542940	-12.5594
K ₂ BiAu-mp1084770	12.5432
ZrS ₂ -mp1186	-12.528
Rb(GeAs) ₃ -mp1192510	-12.5073
HfTl ₂ Se ₃ -mp1102545	-12.4951
Rb ₂ S-mp8041	12.4915
Tl ₄ SiSe ₄ -mp28334	-12.4784
K ₂ CuBr ₃ -mp571440	12.4649
Tb ₇ RhBr ₁₂ -mp1189645	-12.4637
Na ₅ SiAs ₃ -mp18139	12.4617
Na ₆ GaP ₃ -mp1173850	12.4461
Rb ₂ Te ₅ -mp31002	-12.4419
TaI ₅ -mp570679	-12.439

Material	band gap Pressure Coefficient (meV/kB)
$\text{Bi}_3(\text{TeCl}_5)_2$ -mp1193877	-12.4158
Tl_2PAuS_4 -mp9510	-12.3913
$\text{K}_3\text{Nb}_2\text{Se}_{11}$ -mp28428	-12.3893
$\text{Tl}_2\text{Ge}_2\text{Se}_5$ -mp540818	-12.3678
YTITe_2 -mp1065514	-12.2823
K_4ZnP_2 -mp11719	12.2259
TlPt_2S_3 -mp9272	-12.1989
SbSCl_9 -mp557809	-12.1871
$\text{Al}(\text{ICl}_2)_3$ -mp672352	-12.1854
PdBr_2 -mp27857	-12.1801
$\text{K}_2\text{Cu}(\text{PS}_3)_3$ -mp559644	-12.1655
Rb_2Te -mp441	12.1624
$\text{Pt}(\text{PbO}_2)_2$ -mp29332	-12.1479
ZrSe_2 -mp2076	-12.1434
$\text{TlSbAs}_2\text{PbS}_6$ -mp1208201	-12.1352
Rb_4SnO_3 -mp756570	12.1291
CaPbI_6 -mp771691	-12.1217
$\text{Er}_7\text{CoI}_{12}$ -mp1105583	-12.1047
K_4HgAs_2 -mp29484	12.1006
$\text{Rb}_6\text{Cl}_4\text{O}$ -mp29468	12.0979
K_7NaGe_8 -mp1211990	12.091
$\text{Ca}_2\text{Sb}_2\text{S}_5$ -mp29284	-12.0881
K_4Sn_9 -mp570900	-12.0836
RbHgSbTe_3 -mp1219595	-12.0753
DyTITe_2 -mp1007908	-12.0478
K_2TeI_6 -mp27688	-12.0435
SnS -mp2231	-12.0406
Na_4SnTe_4 -mp28108	-12.0396
$\text{Cs}_2\text{P}_2\text{Pd}$ -mp1205610	-12.005

Material	band gap Pressure Coefficient (meV/kB)
WBr ₆ -mp28483	-12.0044
Tl ₂ SiSe ₃ -mp14241	-11.9981
TlRe ₃ (S ₂ Cl) ₂ -mp560005	-11.9902
TlAsS ₂ -mp4988	-11.9809
Nb ₃ I ₈ -mp27772	11.9197
Tb ₇ CoI ₁₂ -mp1105706	-11.9134
K ₆ Na ₃ AlSb ₄ -mp541707	11.8905
Sr ₃ SbI ₃ -mp1208807	-11.8664
GaAs-mp2534	11.8656
Sb ₈ (PbS ₅) ₃ -mp22737	-11.8652
TlSb(PSe ₃) ₂ -mp1105142	-11.8594
HgPSe ₃ -mp7293	-11.8518
Cs ₂ PSe ₅ -mp569060	-11.8509
Rb ₃ AgO ₂ -mp553907	11.8253
K ₄ ZnAs ₂ -mp571461	11.8187
Ge ₃ (Te ₃ As) ₂ -mp541312	-11.8074
Rb ₃ LuCl ₆ -mp1209449	11.8036
Rb ₂ PdCl ₆ -mp28145	-11.8002
Sn ₂ S ₃ -mp1509	-11.7927
DyTl(PSe ₃) ₂ -mp1105239	-11.7899
Rb ₂ TeI ₆ -mp28070	-11.7721
TlBi(PSe ₃) ₂ -mp567864	-11.6881
ErTlTe ₂ -mp1007907	-11.6797
Er ₆ NiI ₁₀ -mp1188388	-11.6791
Rb ₄ InSbCl ₁₂ -mp1219602	-11.6694
KTlBr ₄ -mp28048	-11.655
K ₂ NaInP ₂ -mp21511	11.6439
K ₃ Ga ₃ As ₄ -mp567524	11.6009
EuCl ₂ -mp22887	-11.5921

Material	band gap Pressure Coefficient (meV/kB)
SmTlTe ₂ -mp999132	-11.5908
K ₂ NaInSb ₂ -mp505767	11.5757
Tl ₂ PSe ₃ -mp28394	-11.5543
CsTaSe ₃ -mp685607	-11.5286
CsSnSe ₃ -mp1542038	-11.5186
AuCl-mp32780	-11.5113
NiS ₂ -mp1180046	-11.5039
Pd(SCl ₃) ₂ -mp28174	-11.4834
Sr ₃ P ₁₄ -mp1853	-11.4379
GeBr ₂ -mp541610	-11.4322
Ti ₆ Tl ₅ AgSe ₂₇ -mp570021	-11.4312
K ₅ SnAs ₃ -mp16989	11.4099
K ₂ SeBr ₆ -mp23036	-11.4059
Rb ₂ GaAs ₂ -mp15416	11.3956
AuBr-mp505366	-11.3819
TmTlTe ₂ -mp1008561	-11.3749
KSi-mp1217	11.3621
Rb ₆ Br ₄ O-mp30005	11.3592
Si(PbS ₂) ₂ -mp504564	-11.3555
ZrI ₃ -mp570188	-11.3543
ZrP ₂ S ₇ -mp31014	-11.3392
YTl(PSe ₃) ₂ -mp1105136	-11.3203
TaP ₂ Se ₂ Cl ₅ -mp571250	-11.2988
K ₄ Ge(PSe ₃) ₄ -mp1195433	-11.2779
K ₂ PAuS ₄ -mp9509	-11.2622
Ag ₂ GePbS ₄ -mp861942	-11.2575
Cs ₇ NaSi ₈ -mp1199908	11.2299
TbTl(PSe ₃) ₂ -mp1105141	-11.2135
Rb ₂ Se-mp11327	11.1815

Material	band gap Pressure Coefficient (meV/kB)
$K_2NaInAs_2$ -mp21510	11.1629
$RbTaGeS_5$ -mp863022	-11.1581
$Hg_3(SeBr)_2$ -mp31075	-11.1528
$Li_{10}Ge(PSe_6)_2$ -mp721239	-11.1486
$Li_{10}Si(PSe_6)_2$ -mp721253	-11.1318
Na_8TiAs_4 -mp9071	11.1292
In_4SnS_4 -mp646878	11.1081
Cs_2PtBr_6 -mp30062	-11.1001
$HfSe_2$ -mp985831	-11.0668
In_5S_5Br -mp510347	-11.0602
Tl_3AsSe_4 -mp1201566	-11.0465
CuP_4S_3I -mp554724	-11.034
$Rb_2Cr(BrCl)_2$ -mp1219755	-11.0243
PtI_4 -mp669496	-11.0132
$BaAg_2SnSe_4$ -mp569114	-10.9928
$AlAg(PSe_3)_2$ -mp1228964	-10.9902
$K_2Ga_2As_3$ -mp15432	10.9594
$TlIn_5S_6$ -mp505747	10.9049
$Rb_3Sb_2I_9$ -mp1209693	-10.8953
K_2NaAs -mp34127	10.8794
Rb_2PdBr_6 -mp28084	-10.8576
$TlInTe_2$ -mp22791	-10.8527
Tl_2Te_3 -mp29711	-10.8432
Tl_2GeSe_3 -mp14242	-10.785
$CrAg(PSe_3)_2$ -mp1226281	-10.7691
Cs_2NaAlH_6 -mp989642	10.7451
$RbNb_4Ag(PS_{10})_2$ -mp1219639	-10.74
$NbTeI_3$ -mp540924	-10.7365
$SiAg_6HgSe_6$ -mp1219355	10.7348

Material	band gap Pressure Coefficient (meV/kB)
Cs(SbSe ₂) ₂ -mp3312	-10.723
Na ₃ Sb-mp7956	10.6796
SbAsP ₃ -mp569209	-10.6534
Tl ₃ AgTe ₂ -mp650442	-10.6447
Tl ₃ GeTe ₃ -mp17217	-10.6423
TeRhCl-mp22945	-10.6422
MoCl ₆ -mp1221436	-10.641
Tl ₃ SbS ₃ -mp8393	-10.6005
Rb ₃ LiPb ₄ -mp1209665	10.5982
Rb ₅ Ti ₆ AgSe ₂₇ -mp16001	-10.5834
WCl ₄ -mp980949	-10.5642
NaCaAs-mp961685	10.5456
K ₁₁ Cd ₂ Sb ₅ -mp1194660	10.5373
LuTlTe ₂ -mp1017508	-10.526
Rb ₃ Tm ₂ Cu ₄ Br ₁₃ -mp623862	10.518
CsVI ₃ -mp22991	-10.5036
Y ₆ NiI ₁₀ -mp1188535	-10.5035
K ₂ GaAs ₂ -mp15415	10.4982
K ₂ PtCl ₆ -mp23513	-10.4922
ZrHg ₃ (SeBr ₃) ₂ -mp569970	10.4879
HgBr ₂ -mp571558	-10.4851
ZrSe ₃ -mp1683	-10.4673
KAuSe-mp9881	10.419
Cs ₂ PdBr ₆ -mp1205847	-10.4175
K ₂ AsAuS ₄ -mp9511	-10.3994
Nb ₄ P ₂ S ₂₁ -mp1220713	-10.3922
KTa(AgSe ₂) ₂ -mp571288	-10.3775
LiAuS-mp29829	-10.3655
Rb ₂ Hg ₃ Te ₄ -mp29107	-10.3603

Material	band gap Pressure Coefficient (meV/kB)
Na ₁₀ NbGaAs ₆ -mp1221463	10.3427
Al ₂ Te ₅ -mp9254	-10.3309
ZnP ₁₄ Pb-mp1197426	-10.3224
TlGaSe ₂ -mp17254	-10.3172
NdTlSe ₂ -mp568588	-10.3171
Ba ₂ P ₇ Br-mp1105535	-10.3056
PrTl(PSe ₃) ₂ -mp1195020	-10.2884
K ₂ WSe ₄ -mp18138	-10.2666
Tl ₂ S ₅ -mp30520	-10.2536
BSe ₂ -mp1214789	-10.2397
K ₃ Sn ₂ P ₅ S ₁₈ -mp1211845	-10.2149
Ga ₂ PdBr ₈ -mp30945	-10.2131
Cs ₄ FeO ₃ -mp1205381	10.2058
Na ₆ GaAs ₃ -mp1173830	10.2055
In ₄ Te ₃ -mp617281	10.2046
Ba(SbS ₂) ₂ -mp28129	-10.1944
AuSCl ₇ -mp556587	-10.1809
LiAuI ₄ -mp29520	-10.1766
K ₃ In ₂ As ₃ -mp583615	10.169
Ag ₃ AsSe ₃ -mp662599	10.1514
K ₂ Y ₄ Sn ₂ S ₁₁ -mp560785	-10.1365
SnSe-mp691	-10.1275
NaSrAs-mp9775	10.1193
Tl ₃ SiTe ₃ -mp568020	-10.0861
Ba ₄ Sb ₄ Se ₁₁ -mp28238	-10.0826
K ₅ CuAs ₂ -mp14623	10.0685
PrTlSe ₂ -mp999289	-10.067
K ₂ Sn(AsS ₃) ₂ -mp10776	10.0639
Pr ₃ S ₃ N-mp558940	-10.0506

Material	band gap Pressure Coefficient (meV/kB)
AgAuCl ₄ -mp570340	-10.0434
KNb ₂ PS ₁₀ -mp542972	-10.0408
K ₂ Pt-mp1062676	10.0286
Pr ₃ OsI ₃ -mp570779	-10.0203
ZrTl ₂ S ₃ -mp1102830	-10.0137
Tl ₉ SbSe ₆ -mp676274	10.0131
BaNaBi-mp31235	9.9952
Tl ₃ SbSe ₃ -mp4876	-9.9764
K ₃ IO-mp28171	9.9758
K ₂ PtBr ₆ -mp27691	-9.9723
Li ₂ WS ₄ -mp753195	-9.9552
Rb ₃ P ₁₁ -mp1197062	-9.9397
Ga ₂ TeSe ₂ -mp28423	9.9353
TeSe ₂ -mp1217269	-9.9322
ZnTe-mp2176	9.9257
LuNiBi-mp30457	9.9053
In ₂ Te ₅ -mp1197742	-9.8861
NbTlBr ₄ O-mp551826	-9.8804
SbICl ₈ -mp569512	-9.8747
K ₃ CuO ₂ -mp28273	9.8416
K ₂ Te ₂ As-mp29380	-9.8289
K ₂ ZrTe ₃ -mp29602	-9.8276
K ₂ PdCl ₆ -mp23067	-9.7821
Rb ₃ H ₁₂ N ₅ -mp1198991	9.7717
CsAlTe ₃ -mp1189272	-9.7394
K ₂ TeSe ₃ -mp28419	-9.7342
NaInSn ₂ -mp1220784	9.732
K ₆ InP ₃ -mp1224505	9.711
CdPSe ₃ -mp1079559	9.7104

Material	band gap Pressure Coefficient (meV/kB)
SmTlSe ₂ -mp999137	-9.6776
Al(TeCl ₂) ₂ -mp540628	-9.661
KInSnSe ₄ -mp568379	-9.6565
YAsSe-mp1095603	-9.644
Ba(SbSe ₂) ₂ -mp4727	-9.636
LiHoSe ₂ -mp15796	-9.631
RbAuI ₃ -mp568666	-9.623
Sr(InP) ₂ -mp1078973	9.6046
KMgP-mp1018737	9.594
Rb ₂ MoSe ₄ -mp1193232	-9.5881

-
- [1] A. Jain, S. P. Ong, G. Hautier, W. Chen, W. D. Richards, S. Dacek, S. Cholia, D. Gunter, D. Skinner, G. Ceder, *et al.*, Commentary: The materials project: A materials genome approach to accelerating materials innovation, *APL Materials* **1** (2013).